# Balancing Copper-Induced Cytotoxicity with Conjugation Efficiency in "Click" Chemistry of Polymeric Nanoparticles

By

Evan B. Glass

Thesis

Submitted to the Faculty of the

Graduate School of Vanderbilt University

in partial fulfillment of the requirements

for the degree of

MASTER OF SCIENCE

in

Biomedical Engineering

December 15, 2018

Nashville, Tennessee

Approved:

Todd D. Giorgio, Ph.D.

Fiona E. Yull, D.Phil.

# ACKNOWLEDGMENTS

I would like to thank my advisors, Dr. Todd Giorgio and Dr. Fiona Yull, for their support in my research. Thanks to Dr. Giorgio for developing the original research design and for providing guidance throughout. I would also like to thank several members, past and present, of the Giorgio lab. Thank you to Dr. Shirin Masjedi for training with mice, collection of primary macrophages, and general cell culture techniques. Thank you to Stephanie Dudzinski for flow cytometry training and for running countless samples for me. And thank you to Meredith Jackson for the initial training on all the polymer synthesis/purification techniques performed throughout this study. I would also like to thank the various members of Dr. Craig Duvall's lab who share our workspace and help create an amiable workplace environment. Thanks to Bryan Dollinger of the Duvall lab for training on luminescence microscopy and the fluorimeter. Thank you to Dr. Eric Dailing and Dr. Mukesh Gupta for providing general chemistry-related guidance and for answering several questions.

I would also like to thank my family and friends who have been incredibly supportive of my efforts during this project. I want to thank my parents for always inspiring confidence in my research when needed and my brother for reminding me to balance life inside and outside of lab.

Finally, I would like to thank Dr. Don Stec for NMR training and guidance at certain points of the project, and I want to thank Dr. Dmitry Koktysh for training on Dynamic Light Scattering and Fourier transform infrared spectroscopy in the Vanderbilt Institute of Nanoscale Sciences and Engineering (VINSE). This work was supported by the Vanderbilt School of Engineering and the National Institute of Health through NIH RO1 CA214043.

TABLE OF CONTENTS

Page

LIST OF TABLES

Table Page

LIST OF FIGURES

Figure Page

# CHAPTER I

# BACKGROUND

## Polymeric Nanoparticles for Drug Delivery

Drug delivery is an important area of research for treatment of a variety of diseases, including cancer[1], heart disease[2], autoimmune disease[3], and others. Drug delivery technology began in the early 1950s with the development of sustained release mechanisms that primarily focused on transdermal or oral applications[4]. More recently, these technologies are focusing on overcoming biological barriers to allow for targeted delivery to limit systemic side-effects[5]. Over the past 60 years, drug delivery has exploded into a broad field as groups around the world attempt to solve the physicochemical and biological problems associated with treatment. A number of reviews are available detailing these barriers and the many ways they are being addressed[4–9]. In particular, nanotechnology has been considered for drug delivery applications for over 40 years[10,11]. Many treatments involve molecules with physicochemical properties that limit their use *in vivo*. Hydrophobicity is one of the primary obstacles as an estimated 40% of approved drugs consist of molecules with low solubility[12]. Treatments involving oligonucleotides, such as ribonucleic acid interference (RNAi) in gene therapy, are also unable to be freely delivered due to rapid clearance from the body as well as rapid degradation via enzymatic cleavage[13]. To address these challenges, the delivery vehicle can be as important as the therapeutic agent. Targeted delivery can reduce systemic toxicity while also minimizing the required dosage. The successful delivery of rapidly cleared molecules relies on using a carrier, such as nanoparticles. The surfaces of these carriers can be tailored for targeted delivery and

disguised to avoid immune recognition. Metal nanoparticles were among of the first nanocarriers to be applied to biomedical research due to their ease of synthesis and chemical modification[14]. However, metal particles can have many drawbacks, including limited to no biodegradability, increased inflammation associated with smaller particles, and increased reactive oxygen species (ROS) levels due to initiation of the redox cycle[15]. Alternatively, liposomes have been widely studied and several formulations have made it to clinical trials[16–23]. Liposomal particles have been used since the 1980s and have several advantages over other nanocarriers such as biocompatibility, biodegradability, low toxicity, and feasibility of altering pharmacokinetic properties[19,20,24]. The primary drawbacks of liposomes are limited loading efficiency for certain types of drugs, elevated immunogenicity leading to antibody production, and rapid clearance due to accumulation in the reticuloendothelial system (RES)[20,25].

To combat the problems associated with other nanocarriers, polymeric nanoparticles (PNPs) have become popular since they merge many of the advantages of liposomes with a higher degree of controllability[7,23,26–29]. Advanced organic chemistry techniques available allow for the fabrication of particles specifically designed for a wide range of applications[30]. In order to overcome the multiple barriers for effective *in vivo* functions, there is a clear need for nanocarriers that allow for precise control over several characteristics to allow for optimized delivery. PNPs allow for this precise control over a variety of characteristics such as surface chemistry, surface charge, particle size, particle geometry, rate of biodegradability, and many others[26,28]. Furthermore, PNPs can be fabricated from naturally-occurring polymers or synthetic polymers, depending on the design criteria. Natural polymers can be used in scaffolds or nanoparticles and typically include chitosan, hydroxyapatite, gelatin, alginate, or albumin, among others[27,31–33]. While these polymers can be less immunogenic, they are limited in terms of

modification. Synthetic polymers can be tailored for different applications by using monomers with varying properties. Biodegradable nanoparticles can be fabricated using several polymer formulations, including poly(lactic acid) (PLA), poly(glycolic acid) (PGA), and the combined copolymer poly(lactide-co-glycolide) (PLGA)[34]. These biodegradable particles allow for precise control of drug release over time and have a higher loading capacity of hydrophobic drugs compared to liposomes. Similarly, polymeric micelles composed of block copolymers are able to load hydrophobic molecules/drugs in the particle core while maintaining a hydrophilic corona[35]. While these synthetic PNPs may possess increased immunogenicity compared to natural polymers, they are often functionalized with poly(ethylene glycol) (PEG), which increases circulation time, reduces immunogenicity, and prevents protein adsorption[36–39]. By utilizing polymers with unique properties, "smart" PNPs can be developed that respond to different physiological cues, such as pH or temperature[23]. The pH-responsive polymers can be especially powerful for localized delivery in a particular environment (acidic or basic) or to induce endosomal escape and allow for release of a drug inside the targeted cells[27,28,40–43].

Endosomal escape via pH-responsive polymers is especially useful for preserving the functionality of small interfering ribonucleic acid (siRNA). By combining a pH-responsive diblock copolymer core with a PEG corona, a PNP can be developed that will circulate through the vasculature and only release cargo upon endocytosis, thus releasing the siRNA into the cytosol. In order to deliver the therapeutic load in an effective manner, a targeting mechanism is required.

**Targeting Functionalization via "Click" Chemistry**

One of the more robust families of chemical reactions used in biomedical applications is termed "click" chemistry. These reactions encompass a broad range of methods which all adhere to the same criteria: simple reaction conditions, biological compatibility, and biorthogonal reactivity[44]. A major advancement in the field of "click" chemistry was the development of the copper-catalyzed, alkyne-azide "click" reaction (CuAAC). This reaction was developed by two separate groups in the early 2000s and has been used extensively in the past 16 years[45,46]. The reaction conditions only require an alkyne group, an azide group, and a Cu(I) catalyst. However, the most common method uses a "pre-catalyst" Cu(II) salt (such as copper sulfate) in combination with a reducing agent (typically sodium ascorbate) as described by Fokin and Sharpless in 2002[45,47]. The pre-catalyst allows for aqueous reaction conditions in a solvent composed of water and an alcohol (such as methanol or ethanol) that solubilizes the substrates while maintaining the advantageous aqueous solvent[47]. "Click" chemistry is especially useful for functionalizing PNPs since the polymers can be fabricated with a free alkyne or azide group on the outer surface of the particle. A targeting moiety or other molecular decoration can then be functionalized with the other reagent (azide or alkyne) and the two components can be reacted together. The simple, non-harsh reaction conditions even allow for functionalization *in vivo*[48]. "Click" chemistry has been used for particle functionalization, production of synthetic glycopolypeptides[49], modification of biomolecules in living systems[50], and even direct cell membrane alteration[51,52]. Additionally, the "click" reaction can be used in conjunction with other polymerization techniques without affecting the polymer due to the selectivity of the reaction[53]. Overall, these properties make the CuAAC reaction a prime candidate for surface functionalization of PNPs for drug delivery applications.

**Targeting Macrophages for Potential Immunotherapeutic Effects**

Macrophages are an essential part of the innate immune system as they function as a first line of defense and as an antigen-presenting cell to stimulate an adaptive immune response[54]. Macrophages express a spectrum of phenotypes which differ in both function and receptor expression (**Figure 1**). The two extremes of the spectrum are colloquially known as "M1" and "M2" and correspond to inflammatory and wound healing functions, respectively[55]. Additionally, a unique phenotype known as tumor-associated macrophages (TAMs) enhance tumor progression and suppress antitumor responses[56,57]. Macrophages are the most prevalent immune cells in many tumors, including breast and ovarian cancer, while elevated levels of TAMs correlate with poor prognosis and reduced survival[56,58–61]. Recent studies have shown the therapeutic potential for targeting and "reprogramming" the M2-like TAMs to function as M1 inflammatory macrophages and create a natural immune response to the cancer cells[62–65]. Additionally, preliminary evidence reveals that inducing an inflammatory macrophage response can also activate adaptive immunity by presenting antigens to T-cells and inducing CD8+ T-cell infiltration[63,65]. One of the primary challenges for TAM-specific immunotherapy is targeting the therapeutic load to the desired cells. To accomplish this goal, the CD206 macrophage mannose receptor, which is overexpressed on TAMs and other M2 macrophages, is a potentially useful target. Mannose is a sugar comprising a 6-membered ring that can easily be functionalized with an alkyne group that allows for use of the CuAAC reaction to conjugate onto a PNP. In this way,

a PNP designed for delivery to macrophages can be decorated with mannose to allow for preferential targeting to the appropriate macrophage subtype, in this case M2-like TAMs.

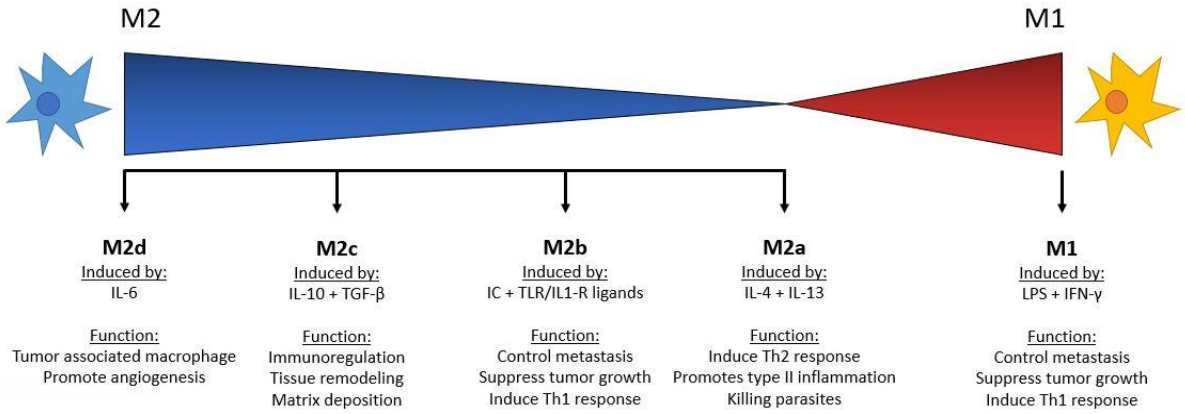


***Figure 1*: Spectrum of Macrophage Phenotypes.** *Macrophages exist across a spectrum of phenotypes, with the two extremes designated "M1" for classically-activated and "M2" for alternatively-activated. There are several subtypes that exist between the ends of the spectrum that have slightly different properties and functions from each other*[55].

# CHAPTER II

# INTRODUCTION

Polymeric nanoparticles, including self-assembling micelles in particular, are commonly used for drug delivery research and have distinct advantages over other nanocarrier formulations, such as metal nanoparticles and liposomes[15,20,25]. Several PNP formulations have been involved in clinical trials with varying levels of success[30,66–68]. The ability to design polymers to provide specific functions, such as biodegradability or pH-responsiveness, which respond to the complex *in vivo* environment makes them an ideal material for the next generation of drug delivery systems. One such application of drug delivery involves delivering siRNA to cells in order to prevent expression of certain proteins. Previously, our lab has developed a novel diblock copolymer that is able to self-assemble into micelles, induce endosomal escape after uptake, and deliver functional siRNA to the cytosol[69,70]. The diblock copolymer core is fabricated using reverse addition-fragmentation chain-transfer (RAFT) polymerization and comprises dimethylaminoethyl methacrylate (DMAEMA) and butyl methacrylate (BMA) monomers, while a poly(ethylene glycol) (PEG) chain forms the corona (PEGDB, **Supplemental Figure 1**). The hydrophobicity of the monomers drives self-assembly into micellar complexes (polyplexes). The tertiary amine in the DMAEMA monomer becomes protonated at low pH and produces a net positive charge that combines with the anionic phosphate groups in nucleotides to aid the self-assembly of the polyplex with siRNA, and thus encapsulate the siRNA in the core of the polyplex. The addition of a PEG corona is intended to minimize protein adsorption, resulting in reduced immunogenicity and increased circulation time. The polyplexes remain stable when elevated to physiological pH due to the hydrophobicity of the polymer. Once the polymers are

endocytosed, the low pH of the late endosome again protonates the tertiary amine of the DMAEMA, which destabilizes the micelle. The hydrophobic polymer chains then insert into the endosomal membrane and induce endosomolysis. The siRNA is released into the cell cytoplasm where it can bind the target messenger RNA (mRNA) and inhibit production of a signaling protein to modify cellular behavior.

To adapt this polymer for use in the CuAAC reaction, the distal end of the PEGDB can be functionalized with an azide group (AzPEGDB). This design allows for PEGDB decoration with an alkyne-modified mannose (propargyl-mannose) via the CuAAC reaction. The resulting polymer is mannose-PEGDB (MnPEGDB). However, the primary drawback of this "click" reaction is the potential for copper-associated toxicity that may result from the copper catalyst[71]. Chelex resin treatment of the post-reaction product is used to remove the copper catalyst, but concern about residual copper has reduced enthusiasm for this reaction in the preparation of materials intended for use in biological systems. The residual copper in CuAAC reaction products, however, has not been quantitatively characterized, creating uncertainties in the potential for toxicity of this polymer formulation. Furthermore, the impact of modulated catalyst concentration on residual copper concentration and "click" reaction efficiency is unknown. A 1 mM $CuSO_4$ concentration is typically used for the CuAAC reaction[72,73], but we hypothesized that by altering the copper catalyst concentration, we could limit the amount of residual copper while also maintaining a high conjugation efficiency of the mannose-alkyne onto the polymer. The ultimate goal of this study was to optimize the "click" conjugation while minimizing cytotoxicity due to residual copper.

# CHAPTER III

# RESULTS AND DISCUSSION

## Synthesis of Mannose-Functionalized Diblock Copolymers

An Azide-PEG-hydroxyl (AzPEGOH) polymer was reacted with a chain transfer agent, 4-cyano-4-(ethylsulfanylthiocarbonyl)-sulfanylpentanoic acid (ECT), to form AzPEGECT, which enabled use of the RAFT polymerization to form AzPEGDB. The AzPEGDB polymer was fabricated using equimolar DMAEMA and BMA and a degree of polymerization of 240. All reaction steps were verified via $^{1}$H-nuclear magnetic resonance (NMR) (**Supplemental Figure 2**). AzPEGDB was reacted with mannose-alkyne via the alkyne-azide "click" reaction to obtain mannose-PEGDB (MnPEGDB) (**Figure 2**).

The "click" reaction (CuAAC) was performed using varying copper catalyst concentrations to examine conjugation efficiency and the amount of residual copper in the polymers as a function of catalyst concentration. Most published studies and CuAAC methods reports use 1 mM copper sulfate in the "click" reaction[72]. When we conduct CuAAC reactions with 1 mM copper sulfate, even with Chelex treatment, the residual copper concentration in the product is over 0.002 mg $Cu^{2+}$ per mg of polymer. In some early studies, treating macrophages with this polymer resulted in a significant decrease in cell viability compared to a control polymer with no exposure to copper (**Supplemental Figure 3**). The potential to prepare low cytotoxicity polymers synthesized using CuAAC reaction chemistry was explored by reducing the copper catalyst concentration. We aim to reduce the residual copper concentration and the

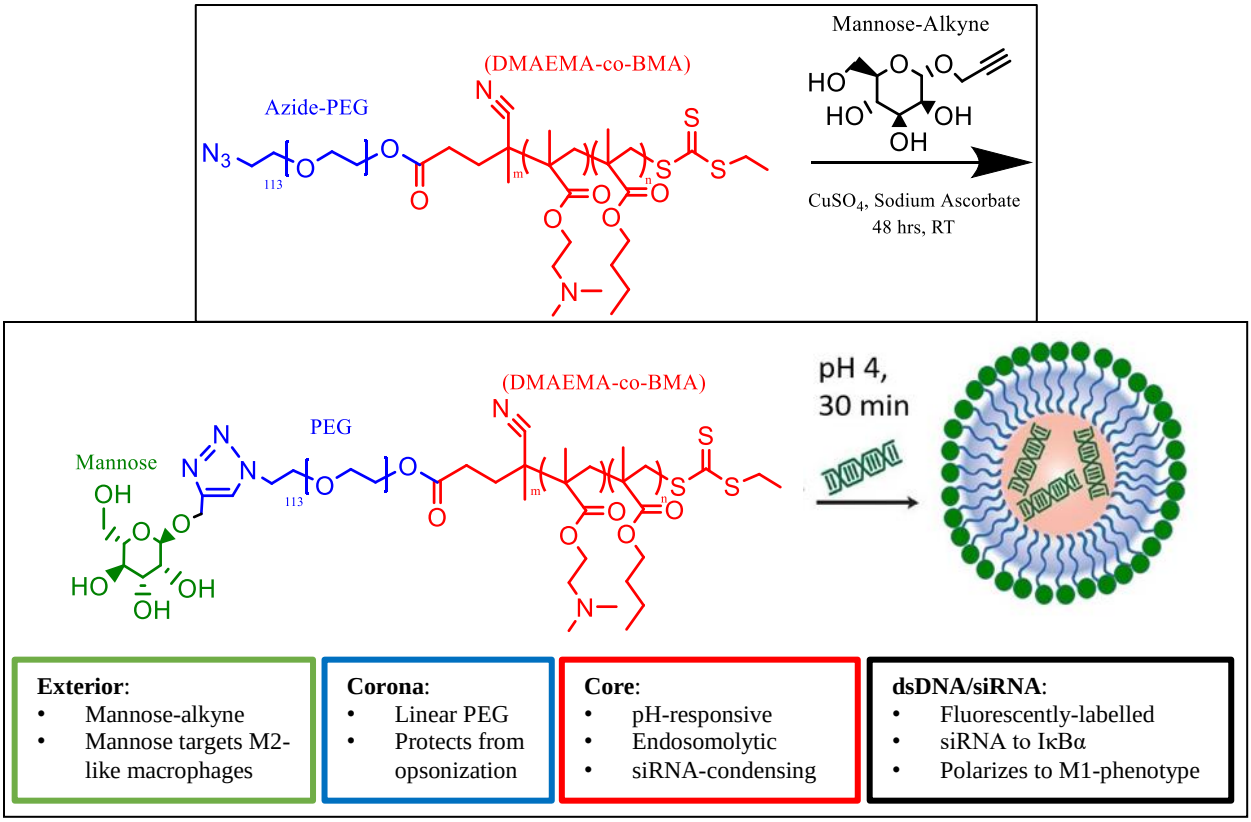


***Figure 2*: "Click" Chemistry Reaction Scheme.** *Schematic representation of the alkyne-azide "click" reaction to conjugate mannose-alkyne onto the corona of the AzPEGDB polymer. The polymer is then complexed with dsDNA to form polyplexes. Figure adapted from Nelson, et al*[69].

associated toxicity while still producing an effective "click" conjugation. To test this hypothesis, we performed the "click" reaction between AzPEGDB and mannose-alkyne with copper concentrations of 0.1, 0.25, 0.5, 0.75, and 1 mM. To verify conjugation of the mannose-alkyne onto the AzPEGDB, Fourier transform infrared (FTIR) spectroscopy was used to examine the change in height of the azide peak at 2100 $cm^{-1}$. Peaks in FTIR spectroscopy are produced by the chemical structures and bonds present in the sample. The peak heights correspond to the prevalence of that bond; so, a change in peak height indicates a change in the concentration of specific functional groups. By quantifying the height of the FTIR peak associated with the azide bond, we characterized the relationship between copper catalyst concentration and the extent of

the CuAAC reaction; the azide peak height will decrease as the efficiency of the ”click” reaction increases, converting the azide bond into a 1,2,3-triazole bond[74,75].

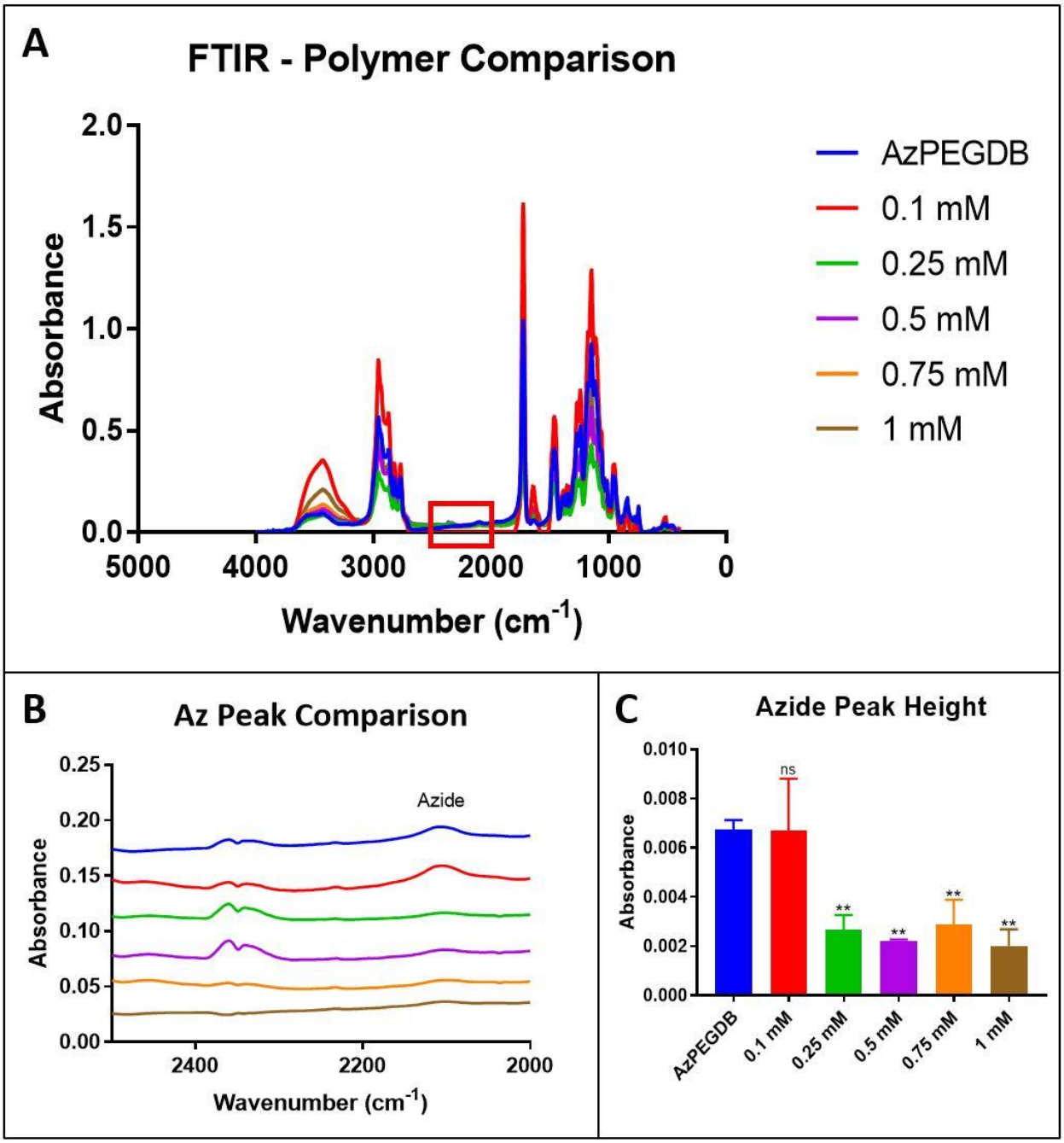


***Figure 3*: FTIR Spectroscopy of “Click” Reaction Polymers.** *(**A**) Whole FTIR spectra for polymers after “click” reaction with various copper catalyst concentrations. (**B**) Detailed view of the azide peaks that are located at 2100 $cm^{-1}$. (**C**) Quantified height of the azide peaks. (**p<0.01 relative to control AzPEGDB).*

By comparing the peak height in the MnPEGDB polymers to that of the precursor AzPEGDB, we estimated the conjugation efficiency of the CuAAC reaction as a function of copper catalyst concentration (**Figure 3**). The lowest concentration of copper catalyst (0.1 mM) did not result in mannose conjugation, but all other concentrations resulted in a significant decrease ($p<0.01$) in azide peak height, suggesting successful "click" reaction. Mannose conjugation was not significantly improved for copper catalyst concentrations above 0.25 mM, which is a four-fold reduction relative to the most commonly reported CuAAC catalyst concentration. After fabrication of the MnPEGDB and removal of residual copper using a Chelex

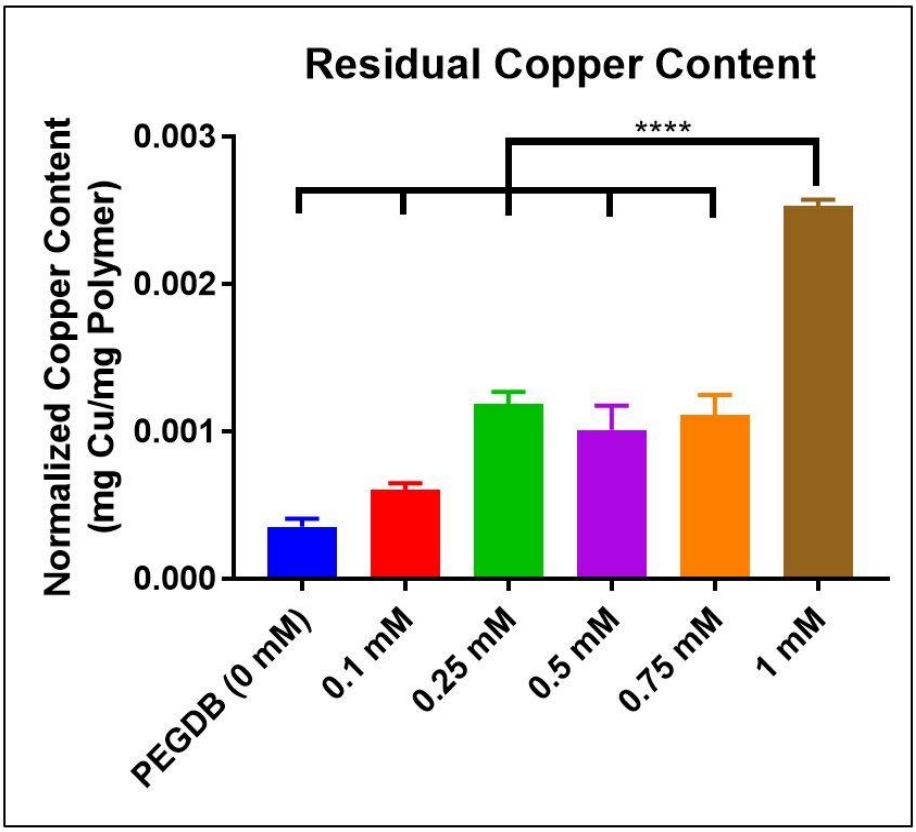


***Figure 4*: $Cu^{2+}$ Assay Quantifying Residual Copper Concentration.** *Copper content, normalized to amount of polymer, was significantly reduced in all polymer groups made with less than 1 mM CuSO4. The concentration of copper for each polymer is: 24 µg/dL in 0.1 mM, 48 µg/dL in 0.25 mM, 40 µg/dL in 0.5 mM, 44 µg/dL in 0.75 mM, and 101 µg/dL in 1 mM. Results normalized as mg Cu2+ per mg polymer. (****p<0.0001 relative to 1 mM group).*

resin following common, previously published conditions[72], the polymers were dissolved in ethanol and molecular grade water. Residual copper was measured using a colorimetric assay that detects $Cu^{2+}$ ions. We normalized the assay results (copper ions in μg/dL) to provide mg of copper per mg of polymer. Residual copper in the final polymer product was significantly reduced for all catalyst concentrations below 1 mM (**Figure 4**). Residual copper concentration for the lowest tested catalyst concentration (0.1 mM) was not significantly different from the PEGDB control polymer, which was not exposed to the CuAAC reaction. Residual copper in the polymers produced using the three middle catalyst concentrations (0.25, 0.5, and 0.75 mM) were not significantly different from each other. Copper catalyst concentrations of 0.25, 0.5, and 0.75 mM support robust 'click' conjugation (**Figure 3C**) and result in significantly reduced residual copper concentrations (**Figure 4**), suggesting that these were among the optimal candidates for synthesis of MnPEGDB intended for use in living systems.

**Formation and Characterization of Mannosylated Polyplexes**

PEGDB self-assembles into micellar complexes (polyplexes) with polynucleotides (siRNA or double stranded DNA (dsDNA)) as previously described[69,72,76]. After formation, polyplexes formed from PEGDB and MnPEGDB were analyzed for size and zeta potential (**Table 1**). Polyplex diameter averaged 146.7 nm with no differences among polymers. The polymer synthesis conditions were selected to produce micelle diameters of approximately 150 nm for eventual efficiency in tumor accumulation after intravenous injection *in vivo*[29,77,78]. The polydispersity index (PDI) for each polymer is less than 0.3, which is below the generally accepted value indicative of a monodisperse solution (0.4-0.5). Zeta potentials for all polymers were not statistically different ($p>0.05$) and were near neutral, which is appropriate for

intravascular administration. Positively-charged particles tend to have higher nonspecific cell uptake as well as shorter blood circulation half-lives[79] while negatively-charged particles hinder cell internalization due to repulsion from the negatively-charged cell membrane surface[80]. Overall, the size and charge characteristics of the polyplexes were appropriate for delivery to the tumor microenvironment from an intravascular route of administration.

***Table 1*: Polyplex Characterization.** *All polymer groups formed polyplexes with similar diameters, low PDIs, and near-neutral zeta potentials.*

| Polymer | Avg Size (d.nm) | PDI | Avg Zeta Potential (mV) |
|---|---|---|---|
| **PEGDB** | 140.4 ± 16.3 | 0.287 | -0.142 ± 0.471 |
| **0.1 mM MnPEGDB** | 145.6 ± 17.6 | 0.273 | -0.111 ± 0.347 |
| **0.25 mM MnPEGDB** | 147.8 ± 16.7 | 0.254 | -0.332 ± 0.398 |
| **0.5 mM MnPEGDB** | 145.1 ± 12.2 | 0.259 | -0.286 ± 0.438 |
| **0.75 mM MnPEGDB** | 150.8 ± 15.6 | 0.262 | 0.249 ± 0.054 |
| **1.0 mM MnPEGDB** | 150.6 ± 13.6 | 0.300 | -0.417 ± 0.430 |

**Examining Cell Viability with Polyplex Treatment**

To examine toxicity of the polymer formulations, immortalized ThP-1 human macrophages and bone marrow-derived macrophages (BMDMs) derived from healthy female FVB mice were cultured. Additionally, human and murine triple negative breast cancer (TNBC) cells lines (MDA-MB-231 and E0771, respectively) and a human epithelial cell line (MCF10a) were also treated with polyplexes to determine cytotoxicity. Human macrophages treated for 24 hours with polyplexes prepared with 0.1 mM or 1.0 mM copper catalyst and loaded with dsDNA length-matched to siRNA (23 base pairs) demonstrated significantly decreased viability relative to untreated controls (**Figure 5A**). The polymer prepared with 1 mM catalyst had the highest amount of residual copper, which is presumed to lead to the observed toxicity. Notably, the 0.1 mM catalyst group, which had the least amount of residual copper, also produced significant toxicity. The FTIR results (**Figure 3**), however, suggest that this polymer had the largest residual

azide peak, indicating the least amount of mannose conjugation and, presumably, the largest number of residual azides on the polymer. Azides are also known to be cytotoxic and we interpret the toxicity of the 0.1 mM polymer to be due to unreacted azides on the AzPEGDB[81]. This interesting observation of azide toxicity has been neglected in previous considerations of

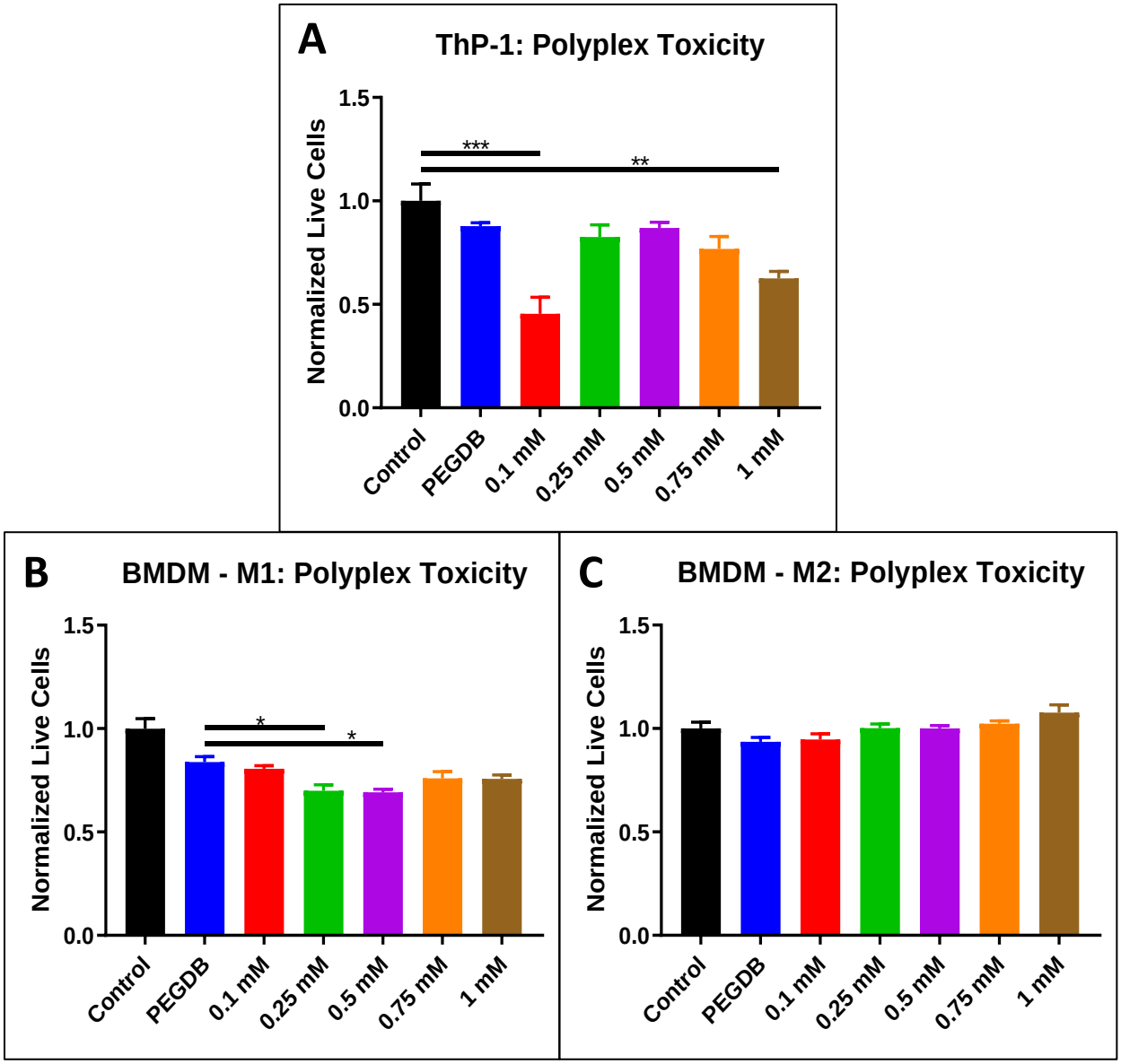


***Figure 5*: Macrophage Toxicity after Polyplex Treatment.** *ThP-1 macrophages and polarized BMDMs were treated with polymer prepared with various copper catalyst concentrations. (**A**) Viability of ThP-1 cells was only significantly decreased in groups made with 0.1 and 1 mM catalyst compared to untreated control (**p<0.01, ***p<0.001) (**B**) M1 polarized BMDMs had significant decreases in viability for all groups compared to control ($p < 0.01$) but only polymers made with 0.25 and 0.5 mM were significantly less than the PEGDB control polymer (*p<0.05). (**C**) M2 polarized BMDMs had no significant changes in viability with any polyplex groups.*

cytotoxicity from CuAAC reaction products, which have focused exclusively on the role of residual copper. Clearly, the optimal copper catalyst concentration is a balance between excess residual copper and relatively few unreacted azides and low residual copper but a greater concentration of remaining cytotoxic azides. Therefore, the optimal catalyst concentration range to limit cell toxicity in human macrophages is between 0.25 and 0.75 mM, which corroborates the results of FTIR and copper content.

To explore the impact of polyplexes on the viability of primary macrophages with varying levels of CD206 expression, BMDMs were cultured with cytokines to polarize them to either an M1 ($CD206_{low}$) or M2 ($CD206_{high}$) phenotype. Interferon-γ (IFN-γ) and lipopolysaccharide (LPS) were added to polarize BMDMs toward M1 and interleukin- (IL-) 4 and IL-13 were used to induce M2 polarization[82]. An additional group of unpolarized BMDMs (M0) were cultured in media with no cytokine treatment. BMDM skewing was characterized via flow cytometry by examining the expression of CD11b and F4/80 (general macrophages markers), CD86 (M1 marker), and CD206 (M2 marker) (**Figure 6**). Following cytokine treatment, we observed significantly higher levels of CD86 in M1 over both M2 and M0 macrophages (**Figure 6E**). Furthermore, we showed that the M2 polarized BMDMs had significantly higher expression of CD206 compared to both M1 and M0, and that the M1 group had a decreased level, though not statistically less, of CD206 compared to the unpolarized macrophages (**Figure 6F**). These results are consistent with the establishment of a $CD206_{low}$ population of M1s and a $CD206_{high}$ population of M2s. M1- and M2-polarized BMDMs were treated with micelles prepared from MnPEGDB and carrying dsDNA as done previously with ThP-1 cells. Polyplex treatment resulted in significant toxicity in the M1 macrophages with all formulations, including the undecorated PEGDB control micelles (**Figure 5B**). Toxicity of

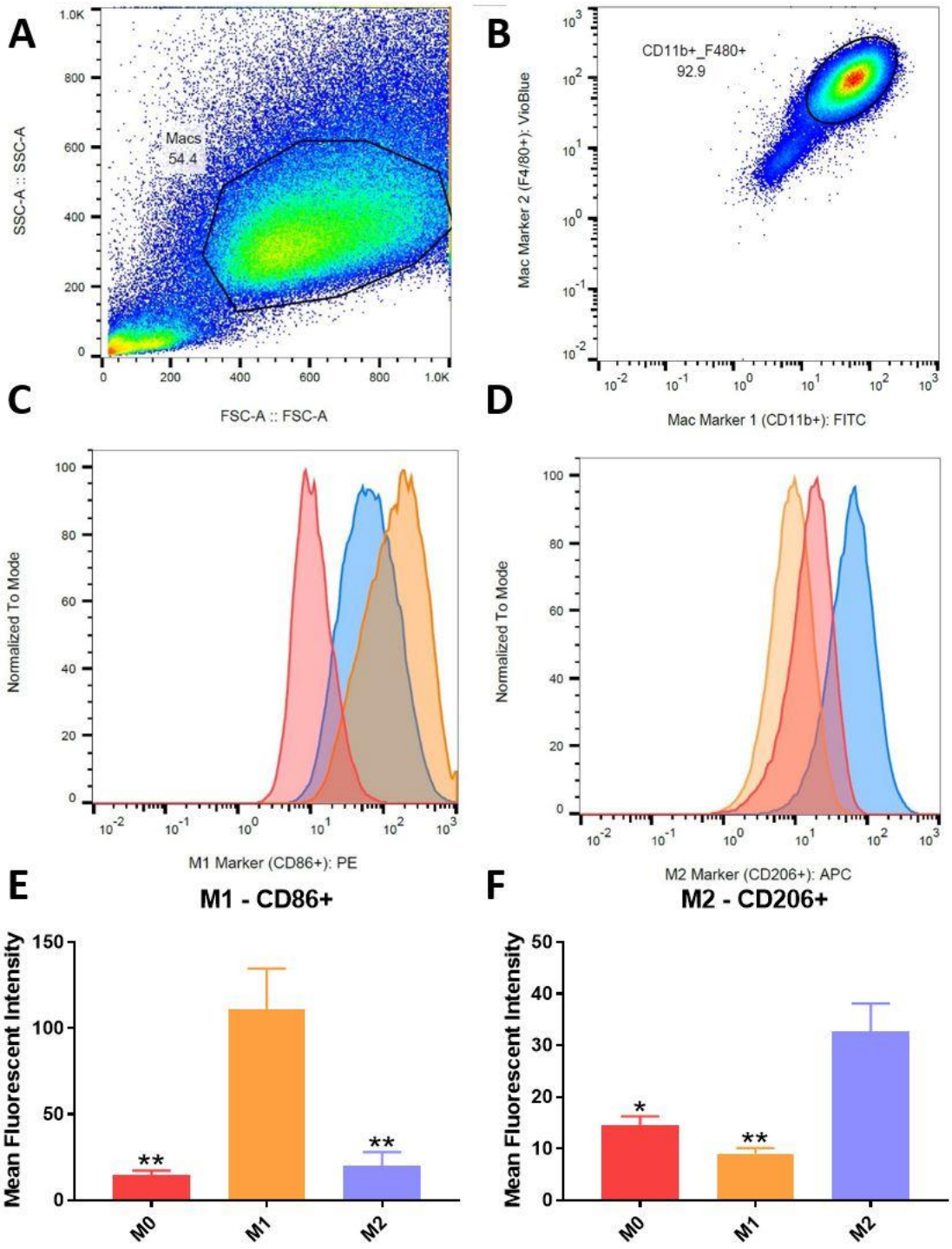


***Figure 6*: Flow Cytometry Analysis of Polarized BMDMs.** *(**A**) Gating of overall cell population in flow cytometry based on side-light scatter intensity vs forward-light scatter intensity. (**B**) Gating of macrophages determined by a double-positive population expressing F4/80 and CD11b. (**C,D**) Histogram plots depicting expressions of M1 (CD86) and M2 (CD206) markers on the different macrophage phenotypes. (**E**) CD86 was significantly increased in the M1-polarized macrophages compared to both M0 and M2 (**p<0.01) (**F**) CD206 was significantly overexpressed in M2 BMDMs (*p<0.05, **p<001).*

MnPEGDB formulations produced with copper catalyst concentrations of 0.1 mM, 0.25 mM or 0.5 mM, but not 0.75 mM or 1.0 mM, was greater than the PEGDB control. This comparison highlights the relative contributions of toxicity from the PEGDB alone relative to the residual azide and copper concentrations in MnPEGDB preparations in M1 polarized macrophages. Additionally, M1 polarized macrophages are known to be inflammatory in nature so nonspecific uptake of the polyplexes could be leading to an inflammatory response. This response can result in mitochondrial-dependent cell death as a response to decreasing inflammatory signals after resolution of the inflammatory response[83]. In contrast to the M1 macrophages, BMDMs polarized to M2 demonstrated no significant decrease in viability due to interaction with micelles prepared from PEGDB or any MnPEGDB preparations (**Figure 5C**). These results are important since the ultimate goal is to target and reprogram M2-like macrophages in the tumor microenvironment, so minimal toxicity in M2 BMDMs provides encouragement for our applications. Additionally, although the same copper-associated toxicity found in ThP-1 macrophages was not observed in the BMDMs, there is still concern for the toxic effects of copper in human macrophages compared to murine macrophages.

Cell viability studies were repeated in human and murine TNBC cell lines and non-tumorigenic human mammary epithelial cells. Tumors prepared from E0771 cells are less aggressive than the well-known and often-used 4T1 model, but possess a similar triple-negative phenotype[84]. MDA-MB-231 cells are a well-established and well-studied TNBC line and display basal-like triple-negative characteristics similar to the E0771 cells[85]. MCF10a cells provide a non-tumorigenic, mammary epithelial control. A murine analog of the MCF10a cells could not be identified among many commercial sources, and a non-tumorigenic murine control is not included in this study. The E0771 cells exhibited similar toxicity for all treatments, although only

polyplexes assembled from the PEGDB or MnPEGDB decorated using 0.5 mM copper catalyst produced toxicity in the E0771 murine breast cancer cells (**Figure 7A**). The other polymers had similar, but no significantly different, toxicity results, which suggests that the cytotoxicity in E0771 cells may be a primary function of the micellar components and not strongly influenced

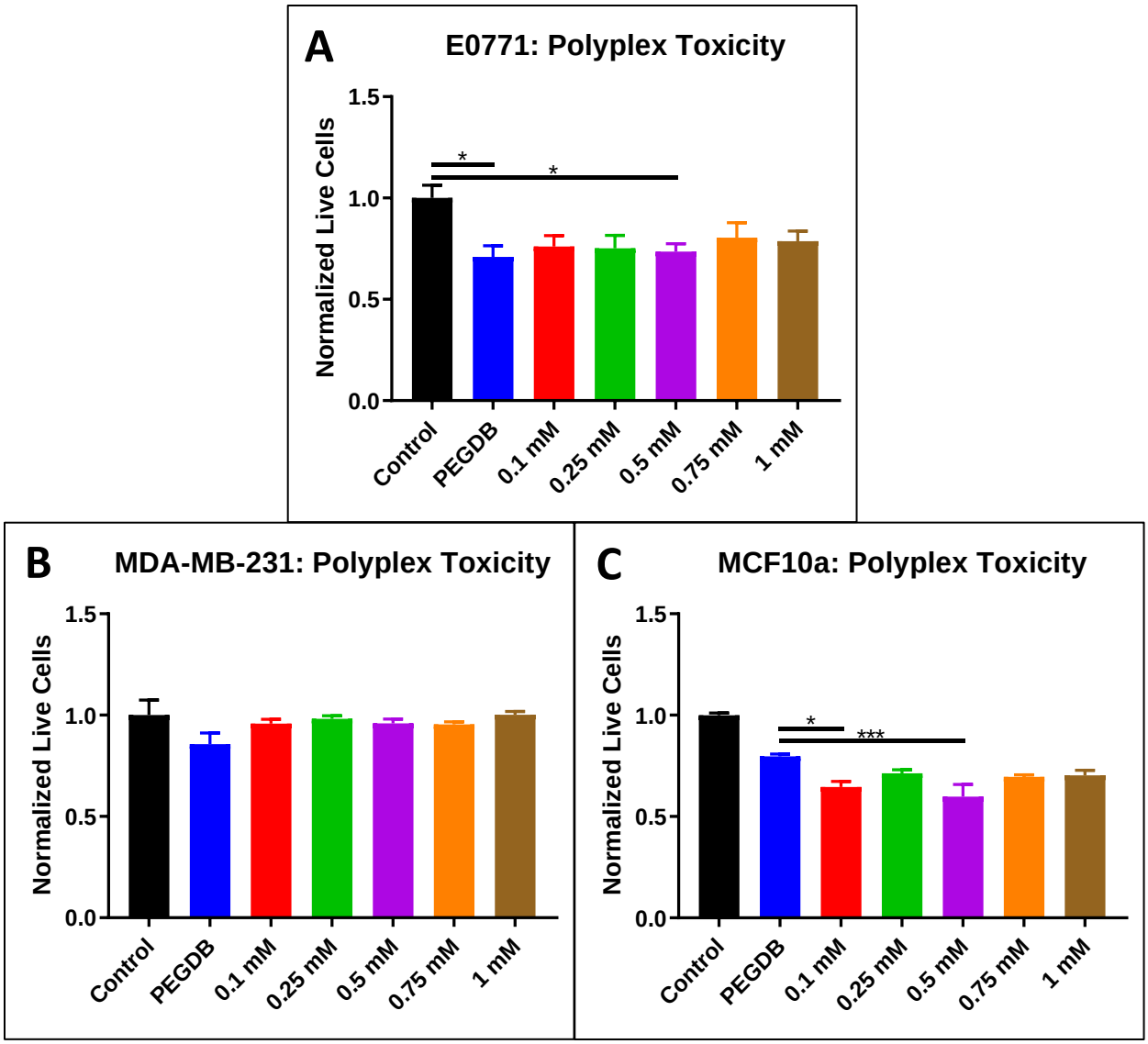


***Figure 7*: Polyplex Toxicity in Mammary TNBC and Epithelial Cells.** *TNBC cells and epithelial cells were treated with polyplexes to examine effects of residual copper on viability. (**A**) E0771 murine cells only showed a significant decrease in viability in the PEG and 0.5 mM groups (*p<0.05) while (**B**) MDA-MB-231 human TNBC cells showed no changes in viability. (**C**) MCF10a human epithelial cells were more sensitive to polyplex treatment with all groups showing significant toxicity from control (p < 0.05), but only the polymers made with 0.1 mM and 0.5 mM copper catalyst were significantly different from the PEG control polymer (*p<0.05, ***p<0.001).*

by copper concentration. MDA-MB-231 cells had no significant changes in viability following treatment with any of the polyplex formulations (**Figure 7B**). Polyplexes prepared at different copper catalyst concentrations generated nearly equal toxicity in MCF10a cells compared to an untreated control, although only the 0.1 mM and 0.5 mM groups were significant compared to the PEGDB control polymer (**Figure 7C**); this result has some similarities with the E0771 outcomes. Overall, the 0.25 mM, 0.75 mM, and 1.0 mM groups had the least effect on viability in both TNBC cell lines and human epithelial cells. These results indicate that the 0.25 mM and 0.75 mM groups are optimal for polymer decoration since polyplexes made from these formulations display limited toxicity in both the targeted cells (macrophages) as well as other cells comprising the tumor microenvironment.

**Copper Salt Cytotoxicity**

Viability studies were conducted with cell culture media containing a known concentration of copper chloride ($CuCl_2$) to examine copper-associated toxicity in the absence of polymers. In general, copper is known to be toxic to cells, but only above a threshold concentration[86]. This study was performed to characterize the lower limits of copper cytotoxicity and inform the selection of CuAAC reaction conditions to enable use of the "click" reactions for *in vitro* or *in vivo* applications. Initially, all of the human cells (ThP-1, MDA-MB-231, MCF10a) were treated with a range of copper concentrations from 0 to 1000 μg/dL. Because the amount of residual copper in the MnPEGDB polymers ranged from 25 to 100 μg/dL, this study would reveal cell viability well beyond this range. The ThP-1 human macrophages showed a trend of decreasing viability as copper concentration increased, but the toxicity was only significant at concentrations of 900 and 1000 μg/dL (**Figure 8A**). However, the trend of decreasing viability

does not start until concentrations above 200 µg/dL, which is well above the highest concentration of copper found in the "click" reaction products. Interestingly, the MDA-MB-231 TNBC cells and the MCF10a epithelial cells showed no significant changes in viability at any of the listed copper concentrations (**Figure 8B,C**), although both cell types did have significant toxicity at even higher concentrations of copper (data not shown). These results would seem to

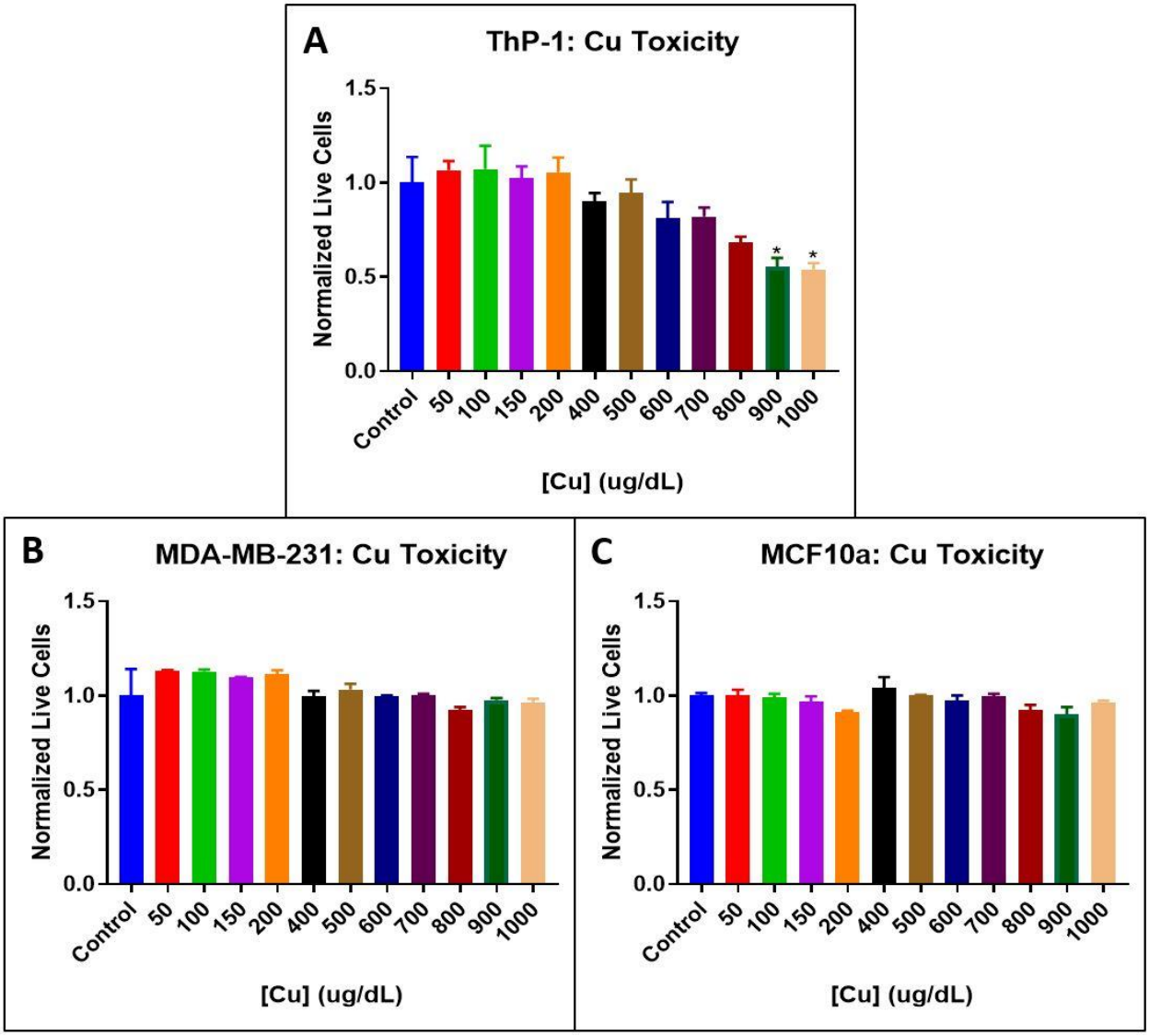


***Figure 8*: Copper Salt Toxicity in Human Cell Lines.** *Human cell lines were treated with various concentrations of $CuCl_2$ for 24 hours to examine $Cu^{2+}$ toxicity. (**A**) ThP-1 macrophages showed a steady decrease in viability as the concentration of copper increased, with the two highest concentrations resulting in a significant decrease (*p<0.05). (**B**) MDA-MB-231 TNBC cells and (**C**) MCF10a epithelial cells both had no significant changes in viability.*

indicate that the toxicity found in the 1 mM polymer group in ThP-1 cells was due to a synergistic effect of both the high residual copper content as well as the micelle itself. However, by reducing the copper content in the other polymer groups, we essentially removed the effects of copper-induced toxicity associated with polyplex treatment.

The same study was repeated in the murine cells (polarized BMDMs, E0771) and revealed similar results in two of the cell types. The E0771 cells showed the same trend of decreasing viability as found in the ThP-1 macrophages, albeit more pronounced. The murine TNBC cells had a significant decrease in cell viability starting at 200 μg/dL, which decreased further as copper concentration was increased (**Figure 9A**). However, similar to before, the decrease in viability occurs at copper concentrations above those found in the polyplexes. The BMDMs revealed perhaps the most intriguing results, with almost all M1 macrophage groups undergoing significant toxicity, while the M2 macrophages had no copper-associated toxicity except at the highest concentration of 1000 μg/dL (**Figure 9B,C**). As hypothesized with regard to polymer toxicity, these results could be due to inflammatory activation of the M1 macrophages leading to an induction of apoptosis due to the high inflammatory cytokine load in the confined wells.

Additional studies, such as examining levels of annexin 5 to check for apoptosis, will be required to determine the effects of macrophage activation *in vitro* and on cell viability. Regardless, these results overall indicate that the toxicity of free copper in cell culture should not limit the use of "click" reaction products since the amount of residual copper in these polymers is well below the concentration range that leads to threshold toxicity in several cell types, including macrophages, TNBC cells, and epithelial cells.

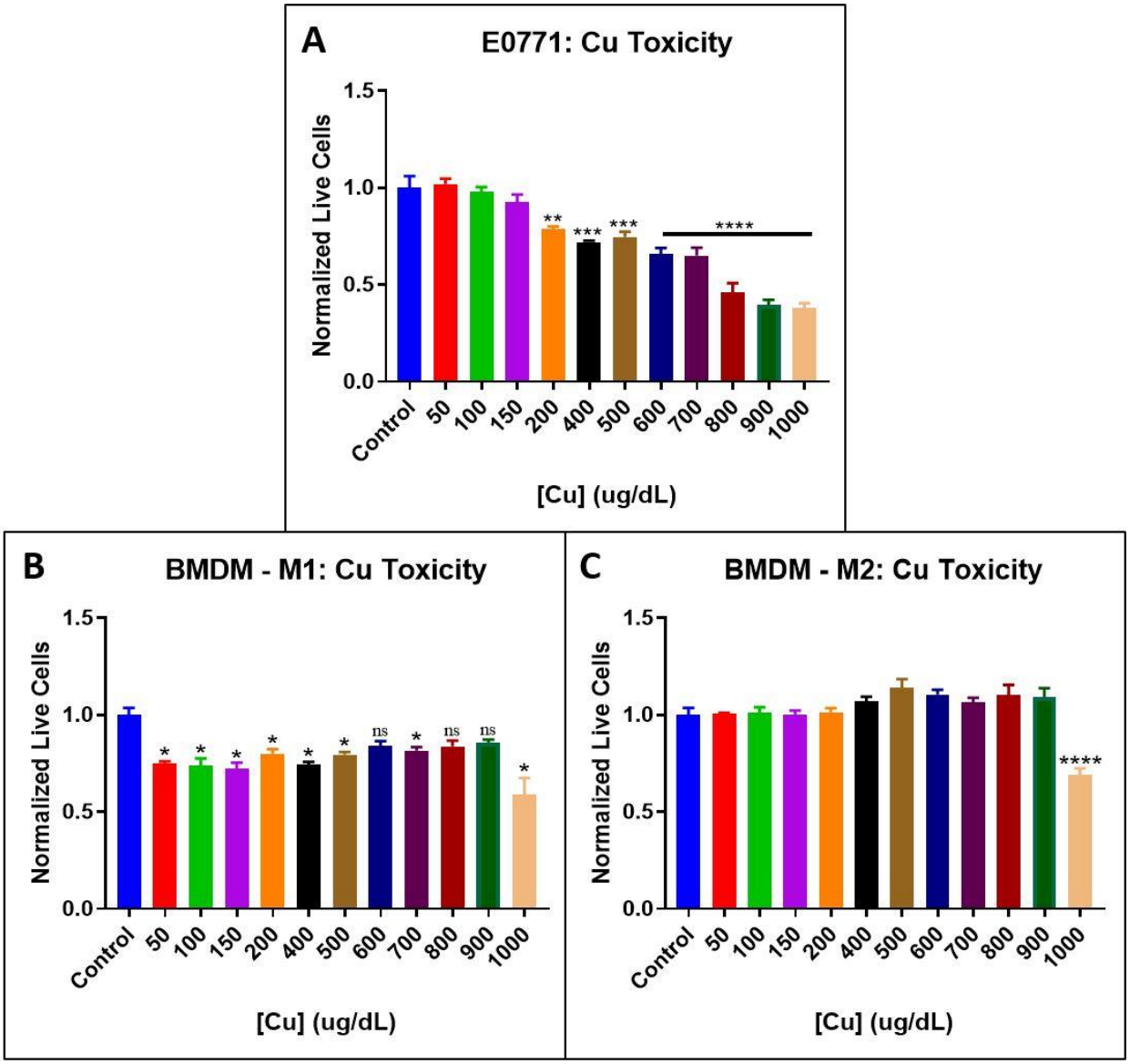


***Figure 9*: Murine Cell Toxicity in Free Copper.** *Free copper toxicity studies were repeated in murine cells. (**A**) E0771 murine TNBC cells resulted in increasing toxicity as $Cu^{2+}$ concentration increased. Significant increase in toxicity was observed starting at 200 µg/dL and became more significant as copper was continually increased (**p<0.01, ***p<0.001, ****p<0.0001). (**B**) M1 polarized BMDMs exhibited significant toxicity at all concentrations except 600, 800, and 900 µg/dL, although there was still a decrease in viability at those concentrations. (**C**) M2 polarized BMDMs displayed no significant toxicity except at the highest concentration of copper treatment.*

**Determining Targeting Efficacy of Mannose-Functionalized Micelles**

The same polyplexes from viability studies were used in an uptake study to evaluate which polymer formulation resulted in the most efficient targeting to $CD206_{high}$ M2 macrophages. Polyplexes were loaded with fluorescently-labelled (Cy5) dsDNA of the same nucleotide length as used previously and incubated with cells. Cell-associated fluorescence intensity was measured at timepoints of one and two hours as an index of polyplex uptake. These timepoints were chosen based on previously published circulation half-lives of similar polyplex formulations[76]. Results were normalized to identical polyplexes formed from non-mannosylated PEGDB controls to assess the effectiveness of targeting surface-expressed CD206. In ThP-1 human macrophages, higher catalyst concentrations from 0.1 mM to 0.75 mM, but not 1 mM, were correlated with greater polyplex uptake, particularly after 2 hours of incubation time (**Figure 10A**). Thus, the greatest uptake was achieved by MnPEGDB micelles prepared from polymers decorated using 0.75 mM of copper catalyst. This result is consistent with our observation of low toxicity from residual copper (**Figure 8A**) in these samples, combined with relatively low residual azides (**Figure 3**). The presence of unreacted azides in this system is presumed to be of elevated importance since the cytotoxic azide groups are converted to conjugated mannose that is predicted to improve polyplex uptake in CD206-presenting cells. Overall, the 0.75 mM group had the greatest increase in normalized fluorescent intensity compared to all other polymer groups at the two-hour timepoint, indicating more efficient delivery of loaded particles to unpolarized ThP-1 macrophages.

Polarized BMDMs were used to examine the effects of CD206 expression on polyplex treatment, this time in terms of uptake. We observed, in viability studies, that micelles induced significant toxicity in M1 polarized, but not M2 polarized, macrophages. In a single cell type,

micellar toxicity is expected to be dose dependent. Extrapolation of this dose-response toxicity to macrophages suggests that M1 polarized BMDMs should demonstrate greater particle uptake than M2 polarized BMDMs. M2 macrophages, however, are associated with more delivered

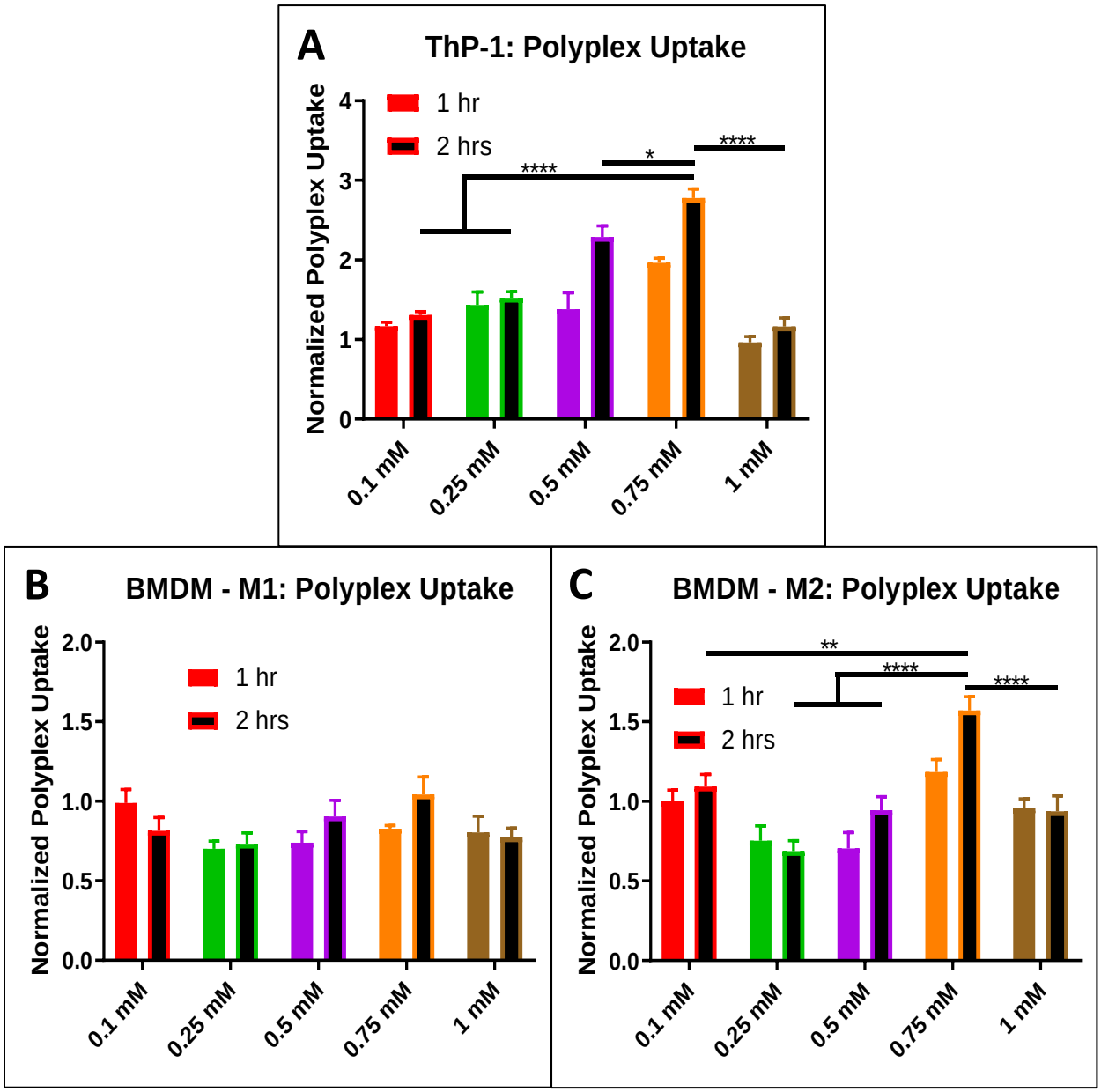


***Figure 10*: Mannose-Associated Uptake of Polyplexes in Macrophages.** *Fluorescent dsDNA-loaded polyplexes were incubated with macrophages for one and two hours, washed, and fluorescence measured. Fluorescence was normalized to the non-decorated control PEGDB. (**A**) ThP-1 human macrophages displayed a significant increase in uptake of the 0.75 mM group at two hours compared to all other polymers (*p<0.05, ****p<0.0001). Experiments were repeated in BMDMs and the (**B**) M1s had no changes in uptake while the (**C**) M2s did display a significant increase in normalized uptake with the 0.75 mM group (**p<0.01, ****p<0.0001).*

dsDNA than M1 polarized macrophages, perhaps as a result of their greater CD206 expression (**Figure 6F**). Mannosylation increases micelle uptake in M2, but not M1, polarized BMDMs (**Figure 10B,C**), consistent with the $CD206_{high}$ and $CD206_{low}$ presentations for M2 and M1 BMDMs, respectively. Thus, the elevated toxicity in M1 polarized BMDMs is not dependent on the intracellular concentration of micelles. Overall, no significant increase in polyplex uptake was observed after two hours of exposure relative to one hour in M1 BMDMs (**Figure 10B**). These findings are consistent with nonspecific endocytosis as the primary mechanism for micelle uptake in M1 macrophages. Additionally, similar to the ThP-1 human macrophages, the polymer made with 0.75 mM catalyst led to the highest amount of uptake in M2 BMDMs at two hours. Even more importantly, this group did not demonstrate a significant change in M1 uptake, consistent with a targeting effect due to mannose decoration. After one hour, the 0.75 mM MnPEGDB micelle uptake was only significantly greater than the 0.25 and 0.5 mM groups, but this result is important since those two groups were the other leading candidates for the optimal mannosylation conditions (**Figure 10**). Furthermore, the 0.75 mM group was the only polyplex to have a normalized uptake greater the 1, indicating preferential targeting over the non-mannosylated control. The 0.75 mM MnPEGDB provided the most significant increase in targeting M2 macrophages, while also not exhibiting a substantial increase in targeting M1 macrophages compared to untargeted control particles. And more importantly, the 0.75 mM group did not result in significant toxicity in human macrophages, an important characteristic that supports the potential for translational activities.

Polyplex association with E0771 murine TNBC cells was slightly increased for polymers made with lower catalyst concentrations (0.1-0.75 mM) although none of these groups were statistically different from each other. The 0.25, 0.5, and 0.75 mM catalyst groups did exhibit

significantly higher normalized uptake than the 1 mM group at the two hour timepoint (**Figure 11A**). For MDA-MB-231 human TNBC cells, only the 0.25 mM group showed a significant increase at two hours (**Figure 11B**). MCF10a epithelial cells demonstrated no differences in uptake as a function of polymer preparation or incubation duration, including in comparison with

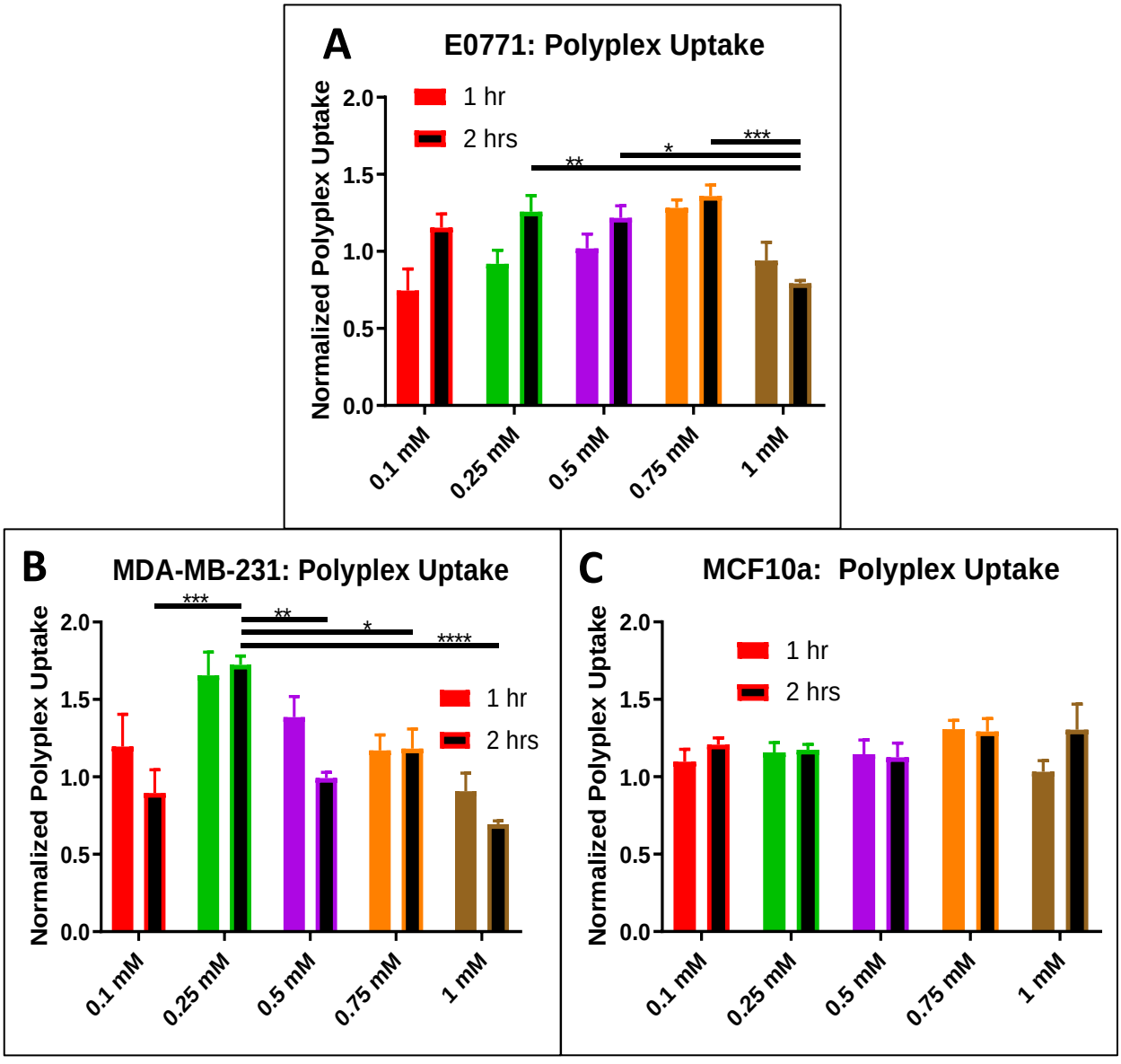


***Figure 11*: Non-specific Polyplex Uptake in Mammary TNBC and Epithelial Cells.** *Uptake studies were repeated in TNBC cells and human epithelial cells. (**A**) E0771 murine TNBC cells showed significant increase in uptake for the middle catalyst concentrations (0.25, 0.5, 0.75 mM) compared to the 1 mM group (*p<0.05, **p<0.01, ***p<0.001). (**B**) MDA-MB-231 cells only showed significant uptake in the polymer made with 0.25 mM copper catalyst compared to all other polymers at two hours (*p<0.05, **p<0.01, ***p<0.001, ****p<0.0001). (**C**) MCF10a cells showed no changes in uptake for any polyplexes.*

the non-mannosylated PEGDB controls (**Figure 11C)** Although it is unclear why some groups demonstrated slight increases in uptake in the TNBC cell lines (0.25, 0.5, and 0.75 in E0771, 0.25 in MDA-MB-231), the group made with 0.75 mM copper catalyst did not result in significant targeting to both human cell lines and only had limited uptake in the murine cells. Taken together with the uptake results in human and murine macrophages, the 0.75 mM copper catalyst produces a polymer that has the most significant increase in targeting M2 polarized macrophages while limiting uptake in all other cell types. It is also interesting to note that in every cell type, the polymer made with 1 mM catalyst had very limited uptake when normalized to the non-decorated control. Although this group was shown to have similar mannose conjugation to the 0.25-0.75 mM catalyst groups (**Figure 3**), there appears to be another factor preventing the mannose from increasing M2 macrophage specificity. While this extraneous factor is presumed to be the excess residual copper, additional studies will need to be performed to examine this effect. Overall, lack of specificity of the 0.75 mM polymer in two types of TNBC cells as well as in human epithelial cells supports the earlier data that this is the optimal catalyst concentration to use in the "click" reaction for producing a polyplex capable of preferentially targeting M2-like macrophages.

# CHAPTER IV

## CONCLUSION and FUTURE DIRECTIONS

In this study, a range of 5 copper catalyst concentrations were examined to optimize polymer conjugation via the alkyne-azide "click" reaction while also minimizing the amount of residual copper that could potentially lead to cell toxicity. We showed that copper catalyst concentrations at or above 0.25 mM had similar conjugation efficiencies of mannose-alkyne onto an azide-functionalized polymer. Additionally, all polymers made with less than 1 mM copper catalyst had a significantly decreased amount of residual copper. We then showed through *in vitro* studies that the decreased amount of copper was able to mitigate the toxicity of the polyplexes when cultured with human macrophages. Although minimal copper-associated toxicity was observed in polarized BMDMs, there was still concern for the toxic effects of copper in human macrophages compared to murine macrophages when using the highest copper catalyst concentration. However, these concerns were alleviated by producing polymers with less residual copper. Reducing the amount of toxicity associated with high residual copper content is important for the potential translational activity of this treatment. Furthermore, we showed that the toxicity directly associated with free copper ions was only significant at a concentration range well above the concentration of copper associated with the products of the CuAAC reaction. These results indicate that although there is slight, non-significant inherent toxicity associated with the polymers, the residual copper from CuAAC reaction products is not in the range to affect cell viability due to copper alone. Finally, the 0.75 mM catalyst group had the highest specificity for M2-polarized BMDMs when normalized to a non-targeted control and compared to all other mannosylated polymer groups. Overall, these results indicate that we

successfully optimized the conjugation efficiency while reducing the amount of residual copper as well as supporting the CuAAC reaction as a powerful, important tool moving forward in the area of developing novel polymeric nanoparticles for *in vivo* applications.

Future work will involve continued use of the 0.75 mM copper catalyst for the "click" reaction, but will instead use other alkyne-functionalized targeting moieties as we strive to further improve targeting to M2 macrophages and, more specifically, TAMs. Sugars such as fucose and sialic acid are also specific for CD206 on M2 macrophages but will not be readily recognized by the general carbohydrate receptors found on cancer cells, thus reducing the amount of off-target uptake[87,88]. These sugars, as well as CD206-specific peptides, will be used for future nanoparticle formulations to compare targeting and immunogenicity to further our abilities to target the unique subset of macrophages found in tumors. Additionally, we will begin to deliver therapeutic siRNA that will lead to beneficial "reprogramming" of the macrophages to an M1 phenotype and examine whether these altered macrophages can successfully target and kill cancer cells while also stimulate the adaptive immune system to induce T-cell activation while also producing long-term memory. This research is also important since it can potentially be used in conjunction with current T-cell targeted immunotherapies which require T-cell infiltration in the tumors to be effective[63].

# CHAPTER V

# MATERIALS and METHODS

## Materials

All materials were purchased from Sigma Aldrich unless otherwise noted. Inhibitors were removed from dimethylaminoethyl methacrylate (DMAEMA) and butyl methacrylate (BMA) using an activated basic aluminum oxide column[69,76]. All DNA and RNA oligonucleotides were purchased from Integrated DNA Technologies (Coralville, IA, USA).

## Synthesis of Mannose-Alkyne

In a 50 mL round bottom flask with a stir bar, 2 g of D-mannose (Mn) was dissolved in 10% (w/v) dimethyl sulfoxide (DMSO). The flask was sealed with a rubber stopper and purged with nitrogen ($N_2$ (g)) for 30 minutes. While purging, triethylamine (TEA) and propargyl bromide were added at a ratio of 60:72:60 moles (mannose:TEA:propargyl bromide). The flask was placed in an oil bath at 40°C on a stir plate and stirred for 24 hours. The solution was extracted into diethyl ether five times to remove excess reagents. The resulting DMSO solution was dissolved in equal volume Nuclease-Free Water (Ambion, AM9932) and extracted into dichloromethane five times to remove other byproducts as well as DMSO. The remaining solution was collected, frozen at -80°C, and lyophilized for two days to obtain solid mannose-alkyne.

**Synthesis of macro-Chain Transfer Agent**

Azide-poly(ethylene glycol)-hydroxyl (AzPEGOH, MW 5000 Da) was purchased from Polysciences, Inc. Synthesis of the chain transfer agent (CTA) 4-cyano-4-(ethylsulfanylthiocarbonyl)-sulfanylpentanoic acid (ECT) has been previously described in detail[89,90]. To fabricate the macro-CTA AzPEGECT, AzPEGOH was dissolved in 5 mL of dichloromethane (DCM). 4-dimethylaminopyridine (DMAP) was added at a 2.5:1 molar ratio DMAP:PEGOH. Separately, ECT was dissolved in 5 mL of DCM at a 5:1 molar excess to PEGOH (accounting for 10 mL total volume when combined). N,N'-dicyclohexylcarbodiimide (DCC) was added to the ECT solution at a 5:1 molar excess to the PEG. The ECT/DCC solution was added to a round bottom flask with a stir bar and a $N_2$ balloon purge was installed. The solution was stirred for 5 minutes to allow the DCC to activate the carboxylic acid group of the ECT. The PEG/DMAP solution was then added. The flask was covered with aluminum foil and stirred for 48 hours at room temperature. The solution was removed and dialyzed with a 3.5 kDa molecular weight cut-off membrane for 24 hours in methanol and an additional, subsequent 24 hours in deionized (DI) water. The resulting solution was frozen at -80°C and lyophilized for 2 days to obtain solid AzPEGECT powder.

**RAFT Polymerization**

Polymerization of the 50%DMAEMA-50%BMA copolymer onto the AzPEGECT was conducted as previously described[69,72,91]. Based on previous experience with the diblock copolymer, we preferred a polymer with approximately 150 monomers[69]. Previous syntheses with similar systems produced a conversion rate of 60-65% so we designed the reaction at a

degree of polymerization of 240. Recrystallized 2,2′-azobis(2-methylpropionitrile) (AIBN) was used as the initiator and added at a ratio of 10:1 CTA:initiator. DMAEMA and BMA were added at 50:50 mol% and the entire solution was placed in a round bottom flask and sealed. The solution was purged with $N_2$ for 30 minutes, covered in aluminum foil, and placed in an oil bath at 70°C for 24 hours. After completion of the reaction, the AzPEG(DMAEMA-co-BMA) (AzPEGDB) solution was dialyzed through a 3.5 kDa dialysis membrane for 24 hours in methanol and 24 hours in DI water. The solution was then frozen at -80°C, lyophilized for 2 days, and stored at -20°C.

**Alkyne-Azide "Click" Functionalization**

AzPEGDB was weighed out and dissolved at 10 mg/mL in 10% (v/v) 200-proof ethanol (EtOH) and 90% Nuclease-Free Water (Ambion). Mannose-alkyne was added at a 1:3 azide:alkyne molar ratio. Additionally, 5 mM of sodium ascorbate was added and the copper catalyst (copper sulfate ($CuSO_4$)) was added at concentrations of 0.1, 0.25, 0.5, 0.75, or 1 mM to examine conjugation efficiency at different catalyst concentrations. The final solution was placed in a 50 mL round bottom flask with a stir bar, sealed with a rubber stopper, and placed on a stir plate at room temperature for 48 hours. After reacting, a Chelex resin (Bio-Rad, 142-1253) was added at 5g/100mL and stirred for 2 hours to remove residual $Cu^{2+}$ ions. The solution was filtered through a 0.45 μm filter to remove the Chelex resin and then placed in 3.5 kDa dialysis membrane and dialyzed in DI water for 24 hours. The final solution was frozen at -80°C, lyophilized for 2 days, and stored at -20°C.

All polymers were characterized using $^{1}H$ nuclear magnetic resonance ($^{1}H$-NMR) spectroscopy (Bruker, 400 MHz), Fourier transform infrared spectroscopy (FTIR, Bruker Tensor 27), and a Copper Assay Kit (Sigma-Aldrich®). All NMR spectra are shown in **Supplemental Figure 2**.

**Polyplex Formation**

All polymeric complexes (polyplexes) were formed as previously described[69,72,76,91]. Initially, polymers were complexed with Cy5-labelled dsDNA for 30 minutes in a 10 mM citrate buffer (pH=4). The solution was restored to pH=7.4 by adding a 10 mM phosphate buffer (pH=8) at 5x volume of the pH 4 solution. Polyplex $N^+$:$P^-$ ratio was determined by mole ratio of protonated amines in DMAEMA polymer (assuming 50% protonation at physiological pH) to the number of phosphates on dsDNA/siRNA. All polyplex treatments were performed at a dose of 50 nM dsDNA with $N^+$:$P^-$ 10:1. Particle size and zeta potential were characterized using a Malvern Zetasizer located in the Vanderbilt Institute of Nanoscale Science and Engineering (VINSE) core facility.

**Cell Culture**

**ThP-1:** ThP-1 human monocytes were cultured in Roswell Park Memorial Institute (RPMI) 1640 medium (Thermo Fisher Scientific, Waltham, MA, USA; 11879-020) supplemented with 10% fetal bovine serum (FBS), 25mM HEPES, 1% penicillin streptomycin (P/S), 1% Minimum Essential Medium (MEM) vitamins, and 4.4 μL β-mercaptoethanol at 37°C in a 5% $CO_2$ humidified atmosphere. To differentiate monocytes into mature macrophages, ThP-1 cells were

plated in the aforementioned media supplemented with 0.1% (v/v) phorbol 12-myristate 13-acetate (PMA) (Thermo Fisher Scientific) and incubated for 4 days to allow for differentiation into mature macrophages[92,93]. Cells were plated in 96-well plates at $1x10^5$ cells/well in 100 µL media. Polyplex or copper salt treatments were added on day 4.

**L929:** L929's were used to produce supplemental media for culturing bone marrow-derived macrophages (BMDMs) taken from mice. L929 murine fibroblasts were cultured in Dublecco's Modified Eagle's Medium (DMEM) (Corning, Inc., Corning, NY, USA; 15-013-CV) supplemented with 10% FBS, 1% L-glutamine, and 1% P/S. L929 cells were grown to confluency in T-175 flasks and 55 mL fresh media was added. On day 7, the media was collected, labeled L929 Week 1 media, and stored at -20°C. A fresh 55 mL media was added, cultured for an additional 7 days, collected, and labeled L929 Week 2 media before being stored at -20°C.

**BMDM:** All animal work was approved by the Vanderbilt University Institutional Animal Care and Use Committee. Healthy female FVB mice were sacrificed at 4-8 weeks of age and the femurs and tibias were extracted. The bone marrow was flushed out with DMEM using a 5 mL syringe and collected in DMEM (Corning; 15-018-CV). The cell suspension was centrifuged (Thermo Scientific, Sorvall ST 8 Centrifuge) at 1000xg for 5 minutes. The old media was aspirated before resuspending the cell pellet in 2 mL ACK (Ammonium, Chloride, Potassium) Lysing Buffer (K•D Medical, RGF-3015) and incubating on ice for 2 minutes to lyse red blood cells. The lysis solution was diluted in 20 mL DMEM and again centrifuged at 1000xg for 5 minutes. The media was aspirated and the resulting BMDMs were resuspended in 10 mL BMDM media: DMEM (15-018-CV) with 10% FBS, 1% P/S, 1% L-glutamine, and 14% 1:1 (v/v) L929 week 1 and week 2 media. The cells were counted by mixing 10 µL cell suspension

with 10 µL Trypan Blue Stain (Life Technologies, 15250-061) and pipetting 10 µL of the resulting mixture into a cell counter slide (Bio-Rad, 145-0011) and running on an Automated Cell Counter (Bio-Rad, TC20$^{TM}$). BMDMs were seeded in 12-well plates at 1x10$^6$ cells/well in 1 mL media or in 96-well plates at 1x10$^5$ cells/well in 100 µL media. To induce M1 and M2 polarization, BMDMs were incubated with M1- or M2-inducing cytokines (**Table 2**)[82].

***Table 2*: BMDM Polarization Protocol.** *BMDMs were cultured using the following protocol, adapted from Ying, et al., to induce M0, M1, and M2 expression*[82].

| Polarization | M0 | M1 | M2 |
|---|---|---|---|
| **Day 0** | Seeded | Seeded | Seeded |
| **Day 2** | Aspirate media, wash with PBS, add fresh media | Aspirate media, wash with PBS, add fresh media | Aspirate media, wash with PBS, add fresh media |
| **Day 4** | Aspirate media, add fresh media | Aspirate media, add fresh media | Aspirate media, add media with 0.01 µg/mL IL-4 and 0.02 µg/mL IL-13 |
| **Day 7** | No treatment | Aspirate media, add media with 0.1 µg/mL IFN-γ and 0.1 ng/mL LPS | No Treatment |
| **Day 8** | Aspirate media and add treatments | Aspirate media and add treatments | Aspirate media and add treatments |

**E0771:** Murine breast cancer cells were used as a comparison to the BMDMs described previously. E0771 cells were cultured in RPMI 1640 (Thermo Fisher Scientific; 11875-093) supplemented with 10% FBS, 1% P/S, and 25 mM HEPES.

**MDA-MB-231:** Human breast cancer cells were used as a comparison to human ThP-1 macrophages. MDA-MB-231 cells were cultured in DMEM (Thermo Fisher Scientific; 11960-044) supplemented with 10% FBS, 1% L-glutamine, and 1% P/S.

**MCF10a:** Human epithelial cells were used as a healthy tissue control for all nanoparticle treatments. MCF10a cells were cultured in Bronchial Epithelial Cell Growth Medium (BEBM) supplemented with a BEBM Bulletkit (Lonza Clonetics; CC-3170 and CC-4175).

**Flow Cytometry**

BMDMs cultured in 12-well plates were polarized following the above protocol. After incubation with the specified cytokines, wells were washed with 0.5 mL PBS and then incubated with 0.5 ml 0.25% Trypsin-EDTA (Life Technologies, 15400-054) for 5 minutes. 1 mL of media was added to each well and cells were repeatedly aspirated with a disposable pipette to dislodge them from the surface and collected in 15 mL conical tubes. Tubes were centrifuged at 1500 rpm for 5 minutes and the supernatant was aspirated. The cell pellet was resuspended in 2 mL of fresh BMDM media and the cells were counted as previously described. Cells were then placed in a 96-well round bottom weight flask at $1x10^6$ cells/well in 300 µL/well. The plate was spun down at 1500 rpm for 5 minutes and "flicked" to remove supernatant without losing cell pellets. An Fc block consisting of 1 µL Fc block (Biolegend, 101320) and 50 µL of flow cytometry (FACS) staining buffer (PBS with 2% FBS) was added to each well. Plates were placed in a 4°C fridge for 10 minutes. A macrophage panel of antibodies consisting of the following was added: CD11b (1:400), F4/80 (1:200), CD86 (1:200), and CD206 (1:200) (Invitrogen). Each antibody was added in 50 µL of FACs buffer so the total volume when calculating the concentrations was in 100 µL per sample. Plates were again placed in the fridge and allowed to stain for 30 minutes in the dark. Plates were spun down at 1500 rpm for 5 minutes and "flicked" to remove supernatant. Each well was resuspended in 200 µL FACS buffer and run on the flow cytometer.

## Viability Assays

**Polyplex Toxicity:** All cell types were plated in 96-well plates for viability assays. BMDMs and ThP-1s were plated at $1x10^5$ cells/well while all other cells were plated at 25,000 cells/well. BMDMs and ThP-1s followed the plating protocols listed above. The other cells types were plated, incubated overnight to allow cells to adhere, and treated with polyplexes. All cells were treated with 50 nM of Cy5-dsDNA loaded into the various polymer formulations. The cells were incubated for 24 hours before conducting a CellTiter-Glo® Luminescence Assay (Promega; G7571). All luminescent results were normalized to the average of the control well luminescence.

**Copper Salt Toxicity:** All cell types were plated as done in polyplex toxicity. $CuCl_2$ was dissolved at 1 mg/ml in 10% (v/v) 200-proof EtOH and media (specific for cell type). This solution was then diluted to a range of 100-1000 µg/dL and 100 µL was added to each well. All cells were incubated for 24 hours before running the CellTiter-Glo® Luminescence Assay.

## Polyplex Uptake

Similar to above, all cells were plated in 96-well plates and treated with 50 nM of Cy5-dsDNA-loaded polyplexes. At timepoints of 1 and 2 hours, the cells were washed 3x with 100 µL PBS and the fluorescence intensity was measured (Tecan Infinite M1000 Pro). All fluorescence results were normalized to the fluorescence of the PEGDB control polyplexes to determine mannose-associated uptake.

## Statistical Analysis

All data presented as mean ± standard error of the mean (SEM). For all FTIR, copper assay, and toxicity studies, a one-way ANOVA with Tukey's post-hoc test was used to compare all groups to all other groups. For all polyplex uptake studies, a two-way ANOVA with Tukey's post-hoc test was used to compare all groups to all other groups at each timepoint, as well as the same groups across timepoints. To establish statistical significance, we used the following: *$p<0.05$, **$p<0.01$, ***$p<0.001$, ****$p<0.0001$.

REFERENCES


1. Dawidczyk, C. M. *et al.* State-of-the-art in design rules for drug delivery platforms: Lessons learned from FDA-approved nanomedicines. *J. Control. Release* **187**, 133–144 (2014).
2. Godin, B. *et al.* Emerging applications of nanomedicine for the diagnosis and treatment of cardiovascular diseases. *Trends Pharmacol. Sci.* **31**, 199–205 (2010).
3. Hunter, Z. *et al.* A biodegradable nanoparticle platform for the induction of antigen-specific immune tolerance for treatment of autoimmune disease. *ACS Nano* **8**, 2148–2160 (2014).
4. Park, K. The Controlled Drug Delivery Systems: Past Forward and Future Back. *J. Control. Release* **190**, 3–8 (2014).
5. Yun, Y. H., Lee, B. K. & Park, K. Controlled Drug Delivery: Historical perspective for the next generation. *J. Control. Release* **10**, 2–7 (2015).
6. Langer, R. Drug delivery and targeting. *Acta Metall.* **392**, 5–10 (1998).
7. Peer, D. *et al.* Nanocarriers as an emerging platform for cancer therapy. *Nat. Nanotechnol.* **2**, 751–760 (2007).
8. Peppas, N. A. Historical perspective on advanced drug delivery: How engineering design and mathematical modeling helped the field mature. *Adv. Drug Deliv. Rev.* **65**, 5–9 (2013).
9. Tiwari, G. *et al.* Drug delivery systems: An updated review. *Int. J. Pharm. Investig.* **2**, 2–11 (2012).
10. Kreuter, J. Nanoparticles-a historical perspective. *Int. J. Pharm.* **331**, 1–10 (2007).
11. Park, K. Facing the truth about nanotechnology in drug delivery. *ACS Nano* **7**, 7442–7447 (2013).
12. Kalepu, S. & Nekkanti, V. Insoluble drug delivery strategies: Review of recent advances and business prospects. *Acta Pharm. Sin. B* **5**, 442–453 (2015).
13. Reischl, D. & Zimmer, A. Drug delivery of siRNA therapeutics: potentials and limits of nanosystems. *Nanomedicine Nanotechnology, Biol. Med.* **5**, 8–20 (2009).
14. Fedlheim, D. L. & Foss, C. A. *Metal Nanoparticles: Synthesis, Characterization, and Applications*. (Marcel Dekker, Inc., 2002).
15. Majdi, A., Aminifard, S. & Zafari, M. Nanotoxicology and nanoparticle safety in biomedical designs. *Int. J. Nanomedicine* **6**, 1117–1127 (2011).
16. Bouchie, A. First microRNA mimic enters clinic. *Nature Biotechnology* **31**, 577 (2013).
17. Duggan, S. T. & Keating, G. M. Pegylated Liposomal Doxorubicin. *Drugs* **71**, 2531–2558 (2011).

18. Koshkaryev, A., Sawant, R., Deshpande, M. & Torchilin, V. Immunoconjugates and long circulating systems: Origins , current state of the art and future directions. *Adv. Drug Deliv. Rev.* **65**, 24–35 (2013).

19. Hua, S. & Wu, S. Y. The use of lipid-based nanocarriers for targeted pain therapies. *Front. Pharmacol.* **4**, 1–7 (2013).

20. Sercombe, L., Veerati, T., Moheimani, F., Wu, S. Y. & Hua, S. Advances and Challenges of Liposome Assisted Drug Delivery. *Front. Pharmacol.* **6**, 1–13 (2015).

21. Allen, T. M. & Cullis, P. R. Liposomal drug delivery systems: From concept to clinical applications. *Adv. Drug Deliv. Rev.* **65**, 36–48 (2013).

22. Pattni, B. S., Chupin, V. V & Torchilin, V. P. New Developments in Liposomal Drug Delivery. *Chem. Rev.* **115**, 10938–10966 (2015).

23. Liu, D., Yang, F., Xiong, F. & Gu, N. The Smart Drug Delivery System and Its Clinical Potential. *Theranostics* **6**, 1306–1323 (2016).

24. Sawant, R. R. & Torchilin, V. P. Challenges in Development of Targeted Liposomal Therapeutics. *AAPS J.* **14**, 303–315 (2012).

25. Szebeni, J. & Moghimi, S. M. Liposome triggering of innate immune responses: A perspective on benefits and adverse reactions. *J. Liposome Res.* **19**, 85–90 (2009).

26. Banik, B. L., Fattahi, P. & Brown, J. L. Polymeric nanoparticles: the future of nanomedicine. *WIREs Nanomed Nanobiotechnol* **8**, 271–299 (2016).

27. El-Say, K. M. & El-Sawy, H. S. Polymeric nanoparticles: Promising platform for drug delivery. *Int. J. Pharm.* **528**, 675–691 (2017).

28. Han, N. *et al.* Development of Surface-Variable Polymeric Nanoparticles for Drug Delivery to Tumors. *Mol. Pharm.* **14**, 1538–1547 (2017).

29. Elsabahy, M. & Wooley, K. L. Design of polymeric nanoparticles for biomedical delivery applications. *Chem. Soc. Rev.* **41**, 2545–2561 (2012).

30. Anselmo, A. C., Prabhakarpandian, B., Pant, K. & Mitragotri, S. Clinical and commercial translation of advanced polymeric nanoparticle systems: opportunities and material challenges. *Transl. Mater. Res.* **4**, 014001 (2017).

31. Swetha, M. *et al.* Biocomposites containing natural polymers and hydroxyapatite for bone tissue engineering. *Int. J. Biol. Macromol.* **47**, 1–4 (2010).

32. Sailaja, A. K., Amareshwar, P. & Chakravarty, P. Different Techniques Used for the Preparation of Nanoparticles Using Natural Polymers and Their Application. *Int. J. Pharm. Pharm. Sci.* **3**, 45–50 (2011).

33. Yang, J., Han, S., Zheng, H., Dong, H. & Liu, J. Preparation and application of micro/nanoparticles based on natural polysaccharides. *Carbohydr. Polym.* **123**, 53–66 (2015).

34. Hans, M. L. & Lowman, A. M. Biodegradable nanoparticles for drug delivery and

targeting. *Curr. Opin. Solid State Mater. Sci.* **6**, 319–327 (2002).

35. Parveen, S., Misra, R. & Sahoo, S. K. Nanoparticles: A boon to drug delivery, therapeutics, diagnostics and imaging. *Nanomedicine Nanotechnology, Biol. Med.* **8**, 147–166 (2012).

36. Veronese, F. M. & Pasut, G. PEGylation, successful approach to drug delivery REVIEWS. *Drug Discov. Today* **10**, 1451–1458 (2005).

37. Cheng, J. *et al.* Formulation of Functionalized PLGA-PEG Nanoparticles for In Vivo Targeted Drug Delivery. *Biomaterials* **28**, 869–876 (2007).

38. Prencipe, G. *et al.* PEG Branched Polymer for Functionalization of Nanomaterials with Ultralong Blood Circulation. *J. Am. Chem. Soc.* **131**, 4783–4787 (2009).

39. Otsuka, H., Nagasaki, Y. & Kataoka, K. PEGylated nanoparticles for biological and pharmaceutical applications. *Adv. Drug Deliv. Rev.* **55**, 403–419 (2003).

40. Sanchez-Sanchez, A., Fulton, D. A. & Pomposo, J. A. PH-responsive single-chain polymer nanoparticles utilising dynamic covalent enamine bonds. *Chem. Commun.* **50**, 1871–1874 (2014).

41. Sharker, S. M. *et al.* pH triggered in vivo photothermal therapy and fluorescence nanoplatform of cancer based on responsive polymer-indocyanine green integrated reduced graphene oxide. *Biomaterials* **61**, 229–238 (2015).

42. Wilson, J. T. *et al.* Enhancement of MHC-I Antigen Presentation via Architectural Control of pH-Responsive, Endosomolytic Polymer Nanoparticles. *AAPS J.* **17**, 358–369 (2015).

43. Zhou, J. *et al.* Characterization and optimization of pH-responsive polymer nanoparticles for drug delivery to oral biofilms. *J. Mater. Chem. B* **4**, 3075–3085 (2016).

44. Astakova, K. *et al.* "Clicking" gene therapeutics: A successful union of chemistry and biomedicine for new solutions. *Mol. Pharm.* **15**, 2892–2899 (2018).

45. Rostovtsev, V. V, Green, L. G., Fokin, V. V & Sharpless, K. B. A Stepwise Huisgen Cycloaddition Process: Copper(I)-Catalyzed Regioselective 'Ligation' of Azides and Terminal Alkynes. *Angew. Chem., Int. Ed.* **41**, 2596–2599 (2002).

46. Tornøe, C. W., Christensen, C. & Meldal, M. Peptidotriazoles on solid phase: [1,2,3]-Triazoles by regiospecific copper(I)-catalyzed 1,3-dipolar cycloadditions of terminal alkynes to azides. *J. Org. Chem.* **67**, 3057–3064 (2002).

47. Liang, L. & Astruc, D. The copper(I)-catalyzed alkyne-azide cycloaddition (CuAAC) 'click' reaction and its applications. An overview. *Coord. Chem. Rev.* **255**, 2933–2945 (2011).

48. Patterson, D. M., Nazarova, L. A. & Prescher, J. A. Finding the Right (Bioorthogonal) Chemistry. *ACS Chem. Biol.* **9**, 592–605 (2014).

49. Kramer, J. R., Onoa, B., Bustamante, C. & Bertozzi, C. R. Chemically tunable mucin chimeras assembled on living cells. *Proc. Natl. Acad. Sci.* **112**, 12574–12579 (2015).

50. McKay, C. S. & Finn, M. G. Click chemistry in complex mixtures: Bioorthogonal bioconjugation. *Chem. Biol.* **21**, 1075–1101 (2014).

51. Luo, W. *et al.* A Dual Receptor and Reporter for Multi-Modal Cell Surface Engineering. *ACS Chem. Biol.* **10**, 2219–2226 (2015).

52. Rogozhnikov, D., Luo, W., Elahipanah, S., O'Brien, P. J. & Yousaf, M. N. Generation of a Scaffold-Free Three-Dimensional Liver Tissue via a Rapid Cell-to-Cell Click Assembly Process. *Bioconjug. Chem.* **27**, 1991–1998 (2016).

53. Ranjan, R. & Brittain, W. J. Combination of Living Radical Polymerization and Click Chemistry for Surface Modification. *Macromolecules* **40**, 6217–6223 (2007).

54. Elhelu, M. A. The role of macrophages in immunology. *J. Natl. Med. Assoc.* **75**, 314–317 (1983).

55. Weagel, E., Smith, C., Liu, P. G., Robison, R. & O'Neill, K. Macrophage Polarization and Its Role in Cancer. *J. Clin. Cell. Immunol.* **6**, 4–11 (2015).

56. Noy, R. & Pollard, J. W. Tumor-Associated Macrophages: From Mechanisms to Therapy. *Immunity* **41**, 49–61 (2014).

57. Condeelis, J. & Pollard, J. W. Macrophages: Obligate partners for tumor cell migration, invasion, and metastasis. *Cell* **124**, 263–266 (2006).

58. Williams, C. B., Yeh, E. S. & Soloff, A. C. Tumor-associated macrophages: unwitting accomplices in breast cancer malignancy. *npj Breast Cancer* **2**, 15025 (2016).

59. Qian, B. Z. & Pollard, J. W. Macrophage Diversity Enhances Tumor Progression and Metastasis. *Cell* **141**, 39–51 (2010).

60. Ojalvo, L. S., King, W., Cox, D. & Pollard, J. W. High-density gene expression analysis of tumor-associated macrophages from mouse mammary tumors. *Am. J. Pathol.* **174**, 1048–1064 (2009).

61. Zabuawala, T. *et al.* An Ets2-Specific Transcriptional Program in Tumor Associated Macrophages Promotes Tumor Metastasis. *Cancer Res.* **70**, (2010).

62. Georgoudaki, A. M. *et al.* Reprogramming Tumor-Associated Macrophages by Antibody Targeting Inhibits Cancer Progression and Metastasis. *Cell Rep.* **15**, 2000–2011 (2016).

63. Guerriero, J. L. *et al.* Class IIa HDAC inhibition reduces breast tumours and metastases through anti-tumour macrophages. *Nature* **543**, 428–432 (2017).

64. Yang, J. *et al.* Myeloid IKKβ Promotes Antitumor Immunity by Modulating CCL11 and the Innate Immune Response. *Cancer Res.* **74**, 7274–7284 (2014).

65. Connelly, L. *et al.* Inhibition of NF-kappa B activity in mammary epithelium increases tumor latency and decreases tumor burden. *Oncogene* **30**, 1402–1412 (2011).

66. Davis, M. E. *et al.* Evidence of RNAi in humans from systemically administered siRNA via targeted nanoparticles. *Nature* **464**, 1067–1070 (2010).

67. Caster, J. M., Patel, A. N., Zhang, T. & Wang, A. Investigational nanomedicines in 2016:

a review of nanotherapeutics currently undergoing clinical trials. *Wiley Interdiscip. Rev. Nanomedicine Nanobiotechnology* **9**, (2017).

68. Matsumura, Y. & Kataoka, K. Preclinical and clinical studies of anticancer agent-incorporating polymer micelles. *Cancer Sci.* **100**, 572–579 (2009).

69. Nelson, C. E. *et al.* Balancing cationic and hydrophobic content of PEGylated siRNA polyplexes enhances endosome escape, stability, blood circulation time, and bioactivity in vivo. *ACS Nano* **7**, 8870–8880 (2013).

70. Werfel, T. A. *et al.* Hydrolytic charge-reversal of PEGylated polyplexes enhances intracellular un-packaging and activity of siRNA. *J. Biomed. Mater. Res. - Part A* **104**, 917–927 (2016).

71. Sletten, E. M. & Bertozzi, C. R. Bioorthogonal Chemistry: Fishing for Selectivity in a Sea of Functionality. *Angew Chem Int Ed Engl.* **48**, 6974–6998 (2009).

72. Yu, S. S. *et al.* Macrophage-specific RNA interference targeting via "click", mannosylated polymeric micelles. *Mol. Pharm.* **10**, 975–87 (2013).

73. Ortega, R. A. *et al.* Biocompatible mannosylated endosomal-escape nanoparticles enhance selective delivery of short nucleotide sequences to tumor associated macrophages. *Nanoscale* **7**, 500–510 (2015).

74. Collman, J. P., Devaraj, N. K., Eberspacher, T. P. A. & Chidsey, C. E. D. Mixed azide-terminated monolayers: A platform for modifying electrode surfaces. *Langmuir* **22**, 2457–2464 (2006).

75. Thode, C. J. & Williams, M. E. Kinetics of 1,3-dipolar cycloaddition on the surfaces of Au nanoparticles. *J. Colloid Interface Sci.* **320**, 346–352 (2008).

76. Jackson, M. A. *et al.* Zwitterionic Nanocarrier Surface Chemistry Improves siRNA Tumor Delivery and Silencing Activity Relative to Polyethylene Glycol . (2017). doi:10.1021/acsnano.7b01110

77. Wang, J. *et al.* The Role of Micelle Size in Tumor Accumulation, Penetration, and Treatment. *ACS Nano* **9**, 7195–7206 (2015).

78. Weissleder, R., Nahrendorf, M. & Pittet, M. J. Imaging macrophages with nanoparticles. *Nat. Mater.* **13**, 125–138 (2014).

79. Alexis, F., Pridgen, E., Molnar, L. K. & Farokhzad, O. C. Factors affecting the clearance and biodistribution of polymeric nanoparticles. *Mol. Pharm.* **5**, 505–515 (2008).

80. Verma, A. & Stellacci, F. Effect of Surface Properties on Nanoparticle-Cell Interactions. *Small* **6**, 12–21 (2010).

81. Jones, J. A., Starkey, J. R. & Kleinhofs, A. Toxicity and mutagenicity of sodium azide in mammalian cell cultures. *Mutat. Res. Toxicol.* **77**, 293–299 (1980).

82. Ying, W., Cheruku, P. S., Bazer, F. W., Safe, S. H. & Zhou, B. Investigation of Macrophage Polarization Using Bone Marrow Derived Macrophages. *J. Vis. Exp.* **76**, 1–8 (2013).

83. Bosca, L., Zeini, M., Traves, P. G. & Hortelano, S. Nitric oxide and cell viability in inflammatory cells: a role for NO in macrophage function and fate. *Toxicology* **208**, 249–258 (2005).

84. Johnstone, C. N. *et al.* Functional and molecular characterisation of EO771.LMB tumours, a new C57BL/6-mouse-derived model of spontaneously metastatic mammary cancer. *Dis. Model. Mech.* **8**, 237–251 (2015).

85. Kathryn, J. C., Sireesha V, G. & Stanley, L. Triple Negative Breast Cancer Cell Lines: One Tool in the Search for Better Treatment of Triple Negative Breast Cancer. *Breast Dis* **32**, 35–48 (2012).

86. Gaetke, L. M., Chow-Johnson, H. S. & Chow, C. K. Copper: Toxicological relevance and mechanisms. *Arch. Toxicol.* **88**, 1929–1938 (2014).

87. Chen, W. C. *et al.* Antigen delivery to macrophages using liposomal nanoparticles targeting Sialoadhesin/CD169. *PLoS One* **7**, 1–9 (2012).

88. Singh, Y. *et al.* Targeting tumor associated macrophages (TAMs) via nanocarriers. *J. Control. Release* **254**, 92–106 (2017).

89. Nelson, C. E. *et al.* Tunable Delivery of siRNA from a Biodegradable Scaffold to Promote Angiogenesis In Vivo. *Adv. Mater.* **26**, 607–506 (2014).

90. Convertine, A. J., Benoit, D. S. W., Duvall, C. L., Hoffman, A. S. & Stayton, P. S. Development of a novel endosomolytic diblock copolymer for siRNA delivery. *J. Control. Release* **133**, 221–229 (2009).

91. Ortega, R. A. *et al.* Manipulating the NF-kB pathway in macrophages using mannosylated, siRNA-delivering nanoparticles can induce immunostimulatory and tumor cytotoxic functions. *Int. J. Nanomedicine* **11**, 2163–2177 (2016).

92. Mittar, D., Paramban, R. & McIntyre, C. *Flow Cytometry and High Content Imaging to Identify Markers of Macrophage Differentiation*. *BD Biosciences* (2011). doi:papers3://publication/uuid/05466CA5-7EF6-409B-8CA3-30840B508BB3

93. Genin, M., Clement, F., Fattaccioli, A., Raes, M. & Michiels, C. M1 and M2 macrophages derived from THP-1 cells differentially modulate the response of cancer cells to etoposide. *BMC Cancer* **15**, 1–14 (2015).

APPENDIX

SUPPLEMENTAL FIGURES

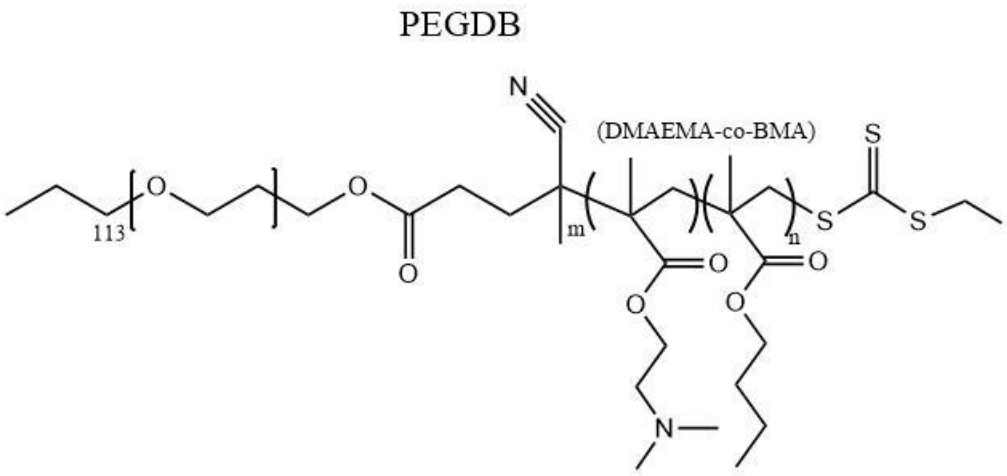


***Supplemental Figure 1*: PEGDB Chemical Structure.** *Structure of undecorated PEGDB used as a control polymer with no exposure to copper.*

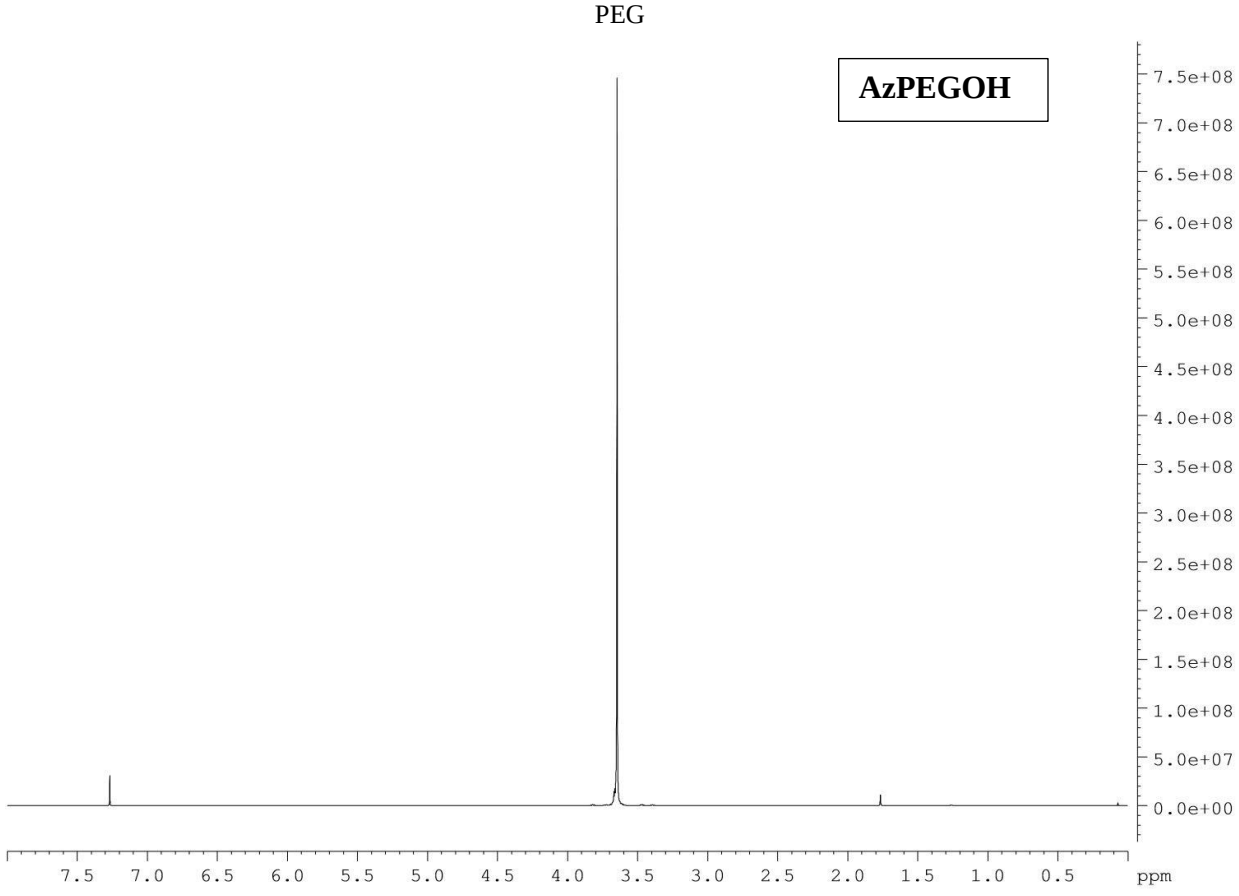

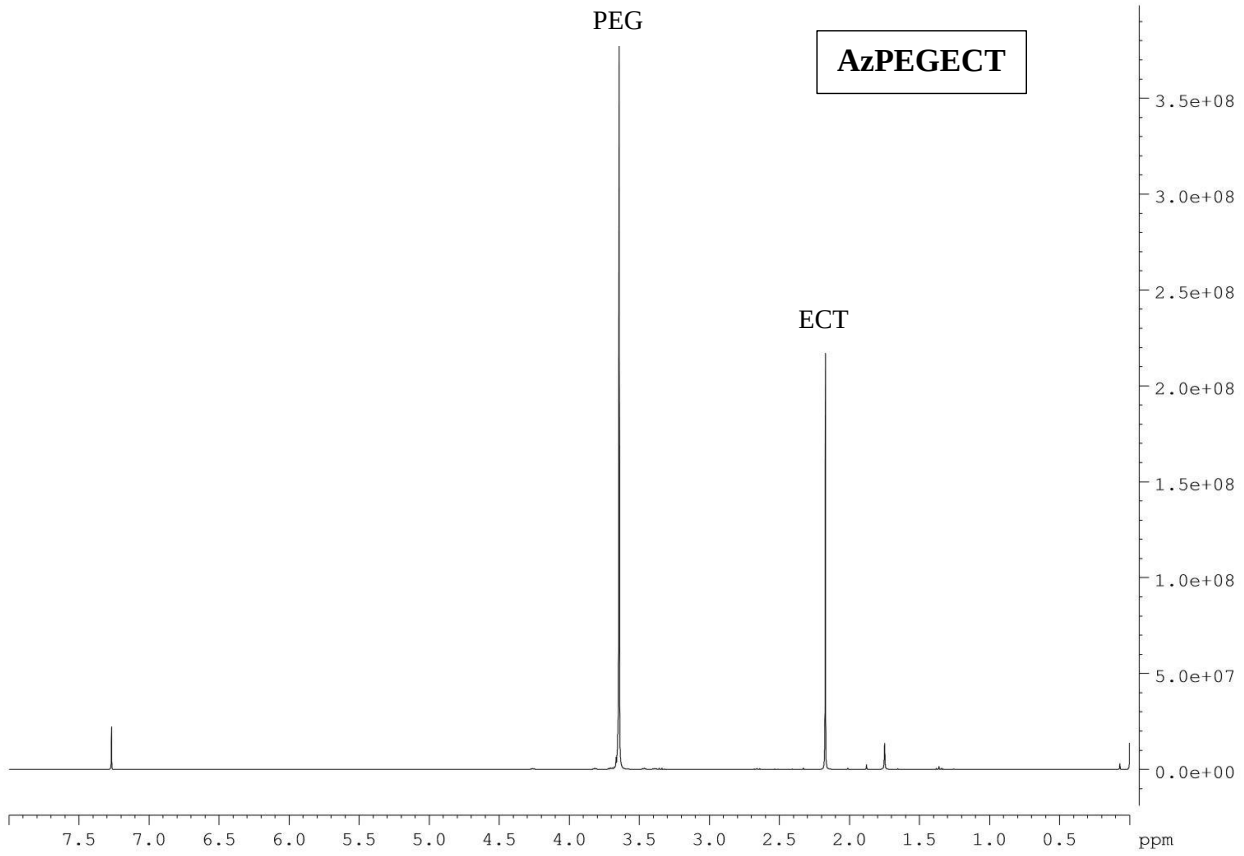
PEG
AzPEGECT
ECT
3.5e+08
3.0e+08
2.5e+08
2.0e+08
1.5e+08
1.0e+08
5.0e+07
0.0e+00
7.5 7.0 6.5 6.0 5.5 5.0 4.5 4.0 3.5 3.0 2.5 2.0 1.5 1.0 0.5
ppm

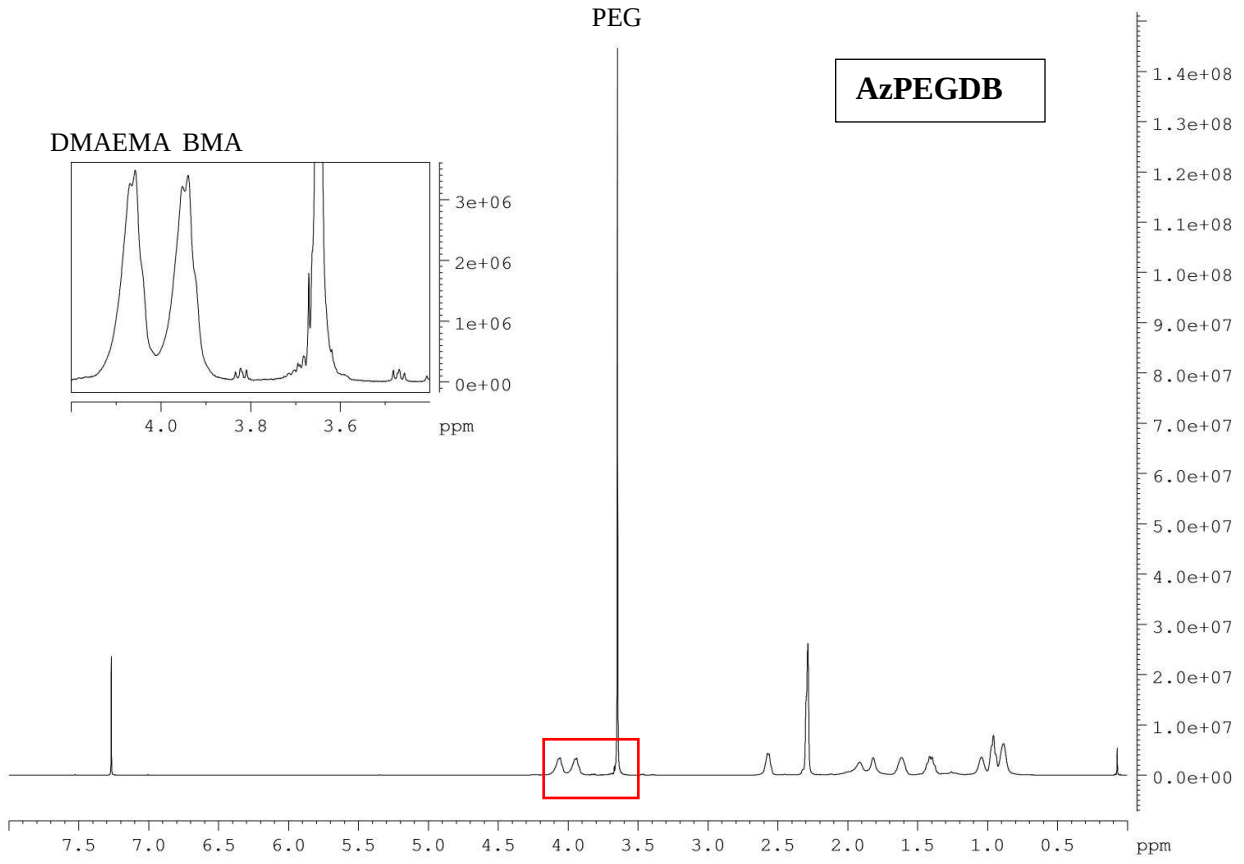
PEG
AzPEGDB
DMAEMA BMA
3e+06
2e+06
1e+06
0e+00
4.0 3.8 3.6
ppm
1.4e+08
1.3e+08
1.2e+08
1.1e+08
1.0e+08
9.0e+07
8.0e+07
7.0e+07
6.0e+07
5.0e+07
4.0e+07
3.0e+07
2.0e+07
1.0e+07
0.0e+00
7.5 7.0 6.5 6.0 5.5 5.0 4.5 4.0 3.5 3.0 2.5 2.0 1.5 1.0 0.5
ppm

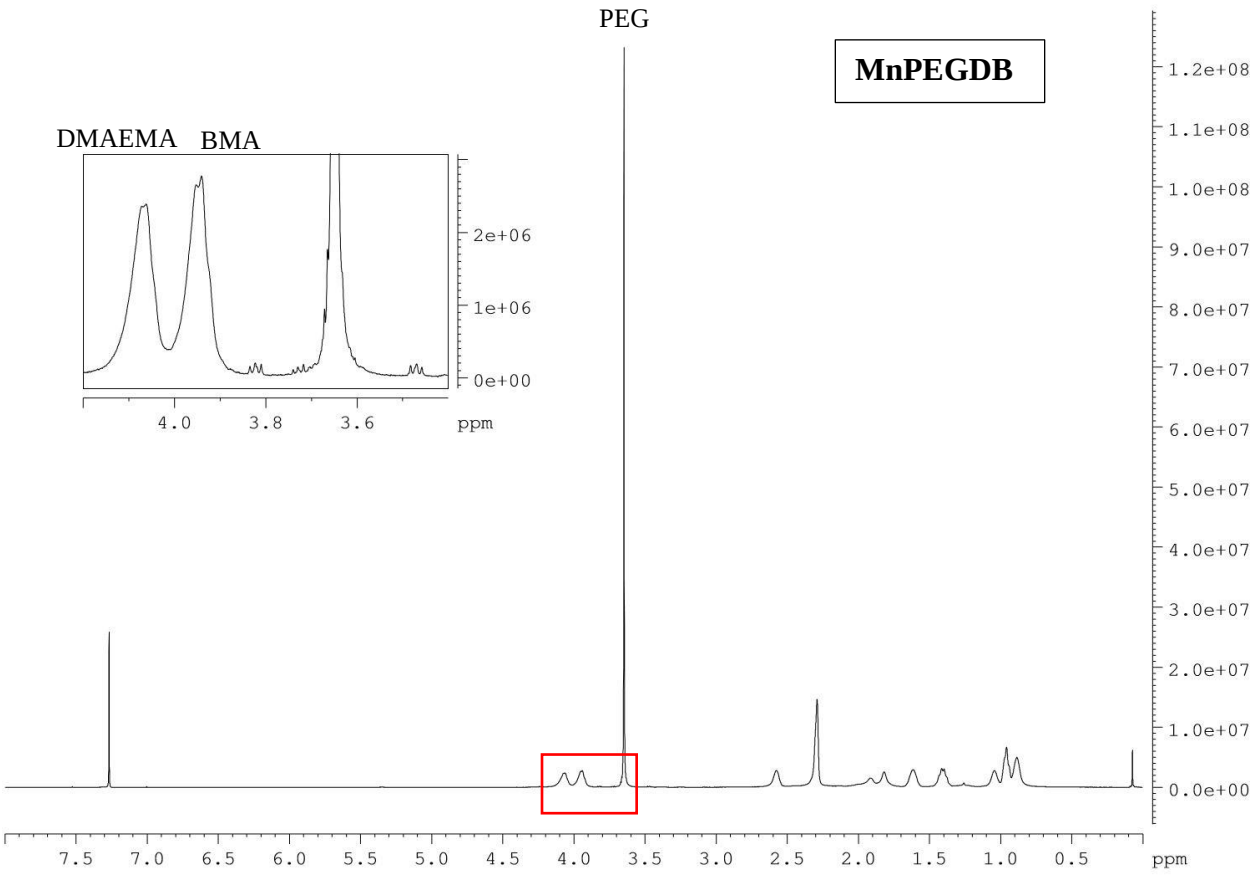


***Supplemental Figure 2*: NMR Spectra for Each Reaction Step.** *Peaks are labelled in each successive figure to indicate a successful reaction. Note that Mannose does not appear in MnPEGDB because the Mannose peaks are located in the same ppm as PEG, DMAEMA, and BMA, but the peaks have a much lower amplitude and therefore are not present in NMR.*

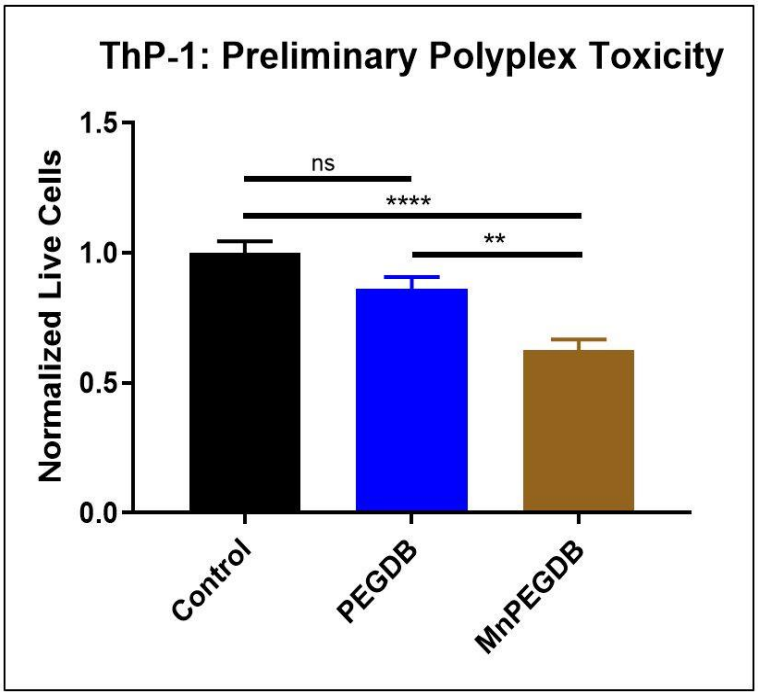


***Supplemental Figure 3*: Preliminary ThP-1 Polyplex Toxicity.** *Initial viability tests revealed a significant decrease in viability when ThP-1 macrophages were treated with MnPEGDB compared to untreated control (****p<0.0001) as well as the control polymer (PEGDB), which has no exposure to copper (**p<0.01).*